RSC Advances

REVIEW

View Article Online
View Journal | View Issue

Cite this: *RSC Adv.*, 2024, **14**, 6823

Recent advances in the role of MXene based hybrid architectures as electrocatalysts for water splitting

Imran Haider Sajid, *[a] Muhammad Z. Iqbal [b] and Syed Rizwan*[a]

The development of non-noble metal based and cost-effective electrocatalysts for water splitting has attracted significant attention due to their potential in production of clean and green hydrogen fuel. Discovered in 2011, a family of two-dimensional transition metal carbides, nitrides, and carbonitrides, have demonstrated promising performance as electro catalysts in the water splitting process due to their high electrical conductivity, very large surface area and abundant catalytic active sites. However, their-long term stability and recyclability are limited due to restacking and agglomeration of MXene flakes. This problem can be solved by combining MXene with other materials to create their hybrid architectures which have demonstrated higher electrocatalytic performance than pristine MXenes. Electrolysis of water encompasses two half-cell reactions, hydrogen evolution reaction (HER) at the cathode and oxygen evolution reaction (OER) at the anode. Firstly, this concise review explains the mechanism of water splitting. Then it provides an overview of the recent advances about applications of MXenes and their hybrid architectures as HER, OER and bifunctional electrocatalysts for overall water splitting. Finally, the recent challenges and potential outlook in the field have been presented. This concise review may provide further understanding about the role of MXene-based hybrid architectures to develop efficient electrocatalysts for water splitting.

Received 3rd October 2023
Accepted 13th February 2024

DOI: 10.1039/d3ra06725d

rsc.li/rsc-advances

Introduction

The ever-increasing global energy demand due to the rapidly growing population of the world has resulted in an energy crisis. The shortage of fossil fuels combined with their negative impacts on the environment has urged researchers to generate green energy from renewable sources. Hydrogen is considered the prospective fuel of the future[1–3] due to its superior gravimetric energy density of 120 MJ kg^{-1}, surpassing gasoline at 44 MJ kg^{-1}. It boasts excellent energy conversion efficiency, environmental friendliness, and emits zero carbon dioxide, producing only water as a byproduct. Hydrogen fuel as green energy has emerged as a promising solution as an alternative energy source.[4–9] The production of hydrogen by electrochemical water splitting has several advantages, including faster reaction time, high purity of the hydrogen produced, and zero greenhouse gas emissions compared to other methods.[10,14] The electrochemical water splitting reaction comprises two half-cell reactions, namely the oxygen evolution reaction (OER) that occurs at the anode and the hydrogen evolution reaction (HER) that takes place at the cathode represented by the following equations.[3,6,11–13]

The usefulness of the electrochemical water splitting depends on stability, efficiency, available active surface area, charge transferability, and cost of the electrocatalyst.[14,15] Electrocatalytic water splitting requires a standard reaction potential of 1.23 V set against the reversible hydrogen electrode (RHE). Practically, due to the sluggish kinetics of HER and OER, the applied potential is much higher than the equilibrium potential. So far, a variety of catalytic and/or photocatalytic semiconductor materials have undergone investigation, encompassing metal oxides, metal nitrides, oxy-nitrides, metal sulfides, alkali metal bases, Z-scheme systems, and organic materials such as carbon and graphene.[16] However, the Electrocatalysts based on noble metals such as platinum (Pt), iridium (Ir), ruthenium (Ru) and their metallic oxides have demonstrated the best performance for water splitting.[15,17–22] The small value of Tafel slope and high exchange current density shown by these precious metal based catalyst are due to their low hydrogen desorption energy and optimum binding energy for hydrogen.[23,24] The industrial use of these efficient electrocatalysts have been limited by their low abundance, high cost and restricted long cycle-ability.[25] A large variety of materials such as transition metals (Co, Fe and Ni) and their oxides, carbides, nitrides and phosphides have been extensively studied as alternative and cost effective catalysts.[26–30] These materials though have exhibited good electrocatalytic

[a]*Physics Characterization and Simulations Lab (PCSL), Department of Physics, School of Natural Sciences (SNS), National University of Sciences and Technology (NUST), Islamabad 44000, Pakistan. E-mail: syedrizwan@sns.nust.edu.pk; ihsajid@gmail.com; Tel: +92 51 886 5599*

[b]*Department of Chemical and Petroleum Engineering, United Arab Emirates University, P.O. Box 15551, Al-Ain, United Arab Emirates*

performance but increase in thickness of active coating, limited active surface area and rapid decline in activity have restricted their overall efficiency.[31–34]

Two-dimensional transition metal carbides,[38] nitrides or carbon nitrides called MXenes have shown promising performance for electrocatalytic water splitting attributed to their exceptionally high electrical conductivity (more than 20 000 S cm^{-1} for Ti_3C_2 film), higher surface area and abundant catalytic active sites.[32] The very first MXene, $Ti_3C_2T_x$ was reported in 2011 by Naguib *et al.* which established a foundation for the discovery of 46 experimentally synthesized and more than 100 theoretically predicted MXenes until the end of 2022.[36–39] MXenes are synthesized by selective etching of A layer atoms (*e.g.*, Si, Al) from their MAX phase precursors which are ternary carbides and nitrides with hexagonal structure. M_n-$X_{n+1}T_x$ is the general formula used to represent MXenes, where M denotes a member of early transition metal (Sc, Mo, Ti, V, Nb, Cr, Hf, Ta, W, Zr) while X could be C, N or CN, T_x represents the surface terminations attached to the surface of outer transition metal layers in terms of elements belonging to group 16 or 17 of the periodic table or imido and hydroxyl groups. The range of values of n extends from 1 to 4 indicating the number of M–X–M layers in a particular MXene and value of x in T_x can be less than or equal to 2.[34,36,40–45] *X* can also represent oxygen as Michalowski *et al.* studied the formation of oxycarbides after the substitution of oxygen in carbide MXenes.[46] The composition space and synthesis of MAX and MXene are shown in Fig. 1. The unique properties of MXenes, along with their straightforward and scalable synthesis methods, make them suitable for investigation in various fields such as energy storage and conversion, electrocatalysis, sensing, electromagnetic interference shielding, wireless communications, structural materials, tribology, environmental remediation, and biomedical applications as depicted in Fig. 2.[37,47–55]

MXenes possess a layered structure, which contributes to their high surface area. The presence of transition metals in MXenes imparts metallic properties and transient electronic states. Additionally, the surface termination groups present in MXenes introduce hydrophilic characteristics. Collectively, these attributes make MXenes highly effective as electrocatalysts for various processes such as hydrogen evolution reaction (HER), oxygen evolution reaction (OER), and overall water splitting.[56]

Although MXene has shown good performance as an electrocatalyst for clean energy conversion reactions, its practical application is seldom viable because it struggles to attain catalytic activity levels comparable to that of commercially available such as Pt, thus creating a significant gap.[7] Supposedly, the most extensively studied type of MXene, $Ti_3C_2T_x$, exhibits suboptimal performance in electrocatalytic water splitting due to unavoidable intersheet aggregation caused by weak van der Waal forces, a high energy barrier for water dissociation, and a strong binding affinity for reaction intermediates. Despite extensive testing for HER activity, bare MXenes present a challenge in effectively combining HER and OER. Consequently, it is deemed essential to develop a stable and efficient bifunctional catalyst for integrated electrochemical water splitting. This necessity arises because OER involves a multi-step reaction route with proton-coupled four electrons transfer, resulting in a dynamically sluggish kinetics and high overpotential compared to the simpler two-electron transfer process of HER. Theoretical studies suggest that modifying the MXene surface through composite construction can alter the electronic structure, lowering HER and OER energy barriers and enhancing electrochemical performance. For instance, Zepeng Lv *et al.* developed an efficient bifunctional electrode material by growing Co2P on $Ti_3C_2T_x$, while Cheng-Feng Du *et al.* enhanced the overall water splitting activity by *in situ* growth of $Ni_{1-x}Fe_xPS_3$ on the MXene surface. Various other approaches have been explored to reinforce the bifunctionality of MXenes, although these methods involve intricate synthesis routes and underlying electrochemical mechanistic pathways.[57]

This review provides an overview of electrocatalysts based on 2D layered MXenes and their hybrid architectures for hydrogen evolution reaction (HER), oxygen evolution reaction (OER) and overall water splitting across various pH conditions. It not only covers recent developments but also includes discussions on the basic mechanism of HER and OER experiments. The "Outlook and Summary" section offers ideas and visions for achieving superior electrocatalytic performance in the field of water splitting, with the purpose of enabling large-scale applications.

Basic reaction mechanism of water splitting

A typical water electrolyzer contains three necessary elements: an electrolyte, a cathode, and an anode. With application of an external voltage greater than the equilibrium voltage required for water splitting, the energy drives the splitting of water molecules. This process results in the production of and oxygen gas through the oxygen evolution reaction (OER) at the anode and hydrogen gas through the hydrogen evolution reaction (HER) at the cathode. Under standard conditions of temperature and pressure (298 K, 1 atm), theoretical value of the equilibrium potential required for water splitting is 1.229 V.[58] The overall reaction for electrolysis of water is $2H_2O \rightarrow 2H_2 + O_2$.

However, a considerable overpotential is needed to overcome the potential loss owing to the sluggish kinetics of the electrochemical reaction involved. Oxygen evolving electrodes exhibit a significantly lower overpotential in alkaline media compared to neutral or acidic media. A higher overpotential is observed in neutral and alkaline conditions for hydrogen evolving electrodes. As a consequence, efficient water-splitting processes often employ exceptionally active electrocatalysts. These catalysts play a vital role in promoting electrochemical reactions on the electrode surfaces, efficiently decreasing energy consumption in the process.[59–61] The successful application of water electrolyzers, which are considered advanced renewable energy devices for transforming intermittent electricity from sustainable sources like wind, solar, and tidal power into fuels, holds significant importance in addressing environmental concerns and the energy crisis. Depending on the membrane materials used in electrolytic cells, water splitting can occur through

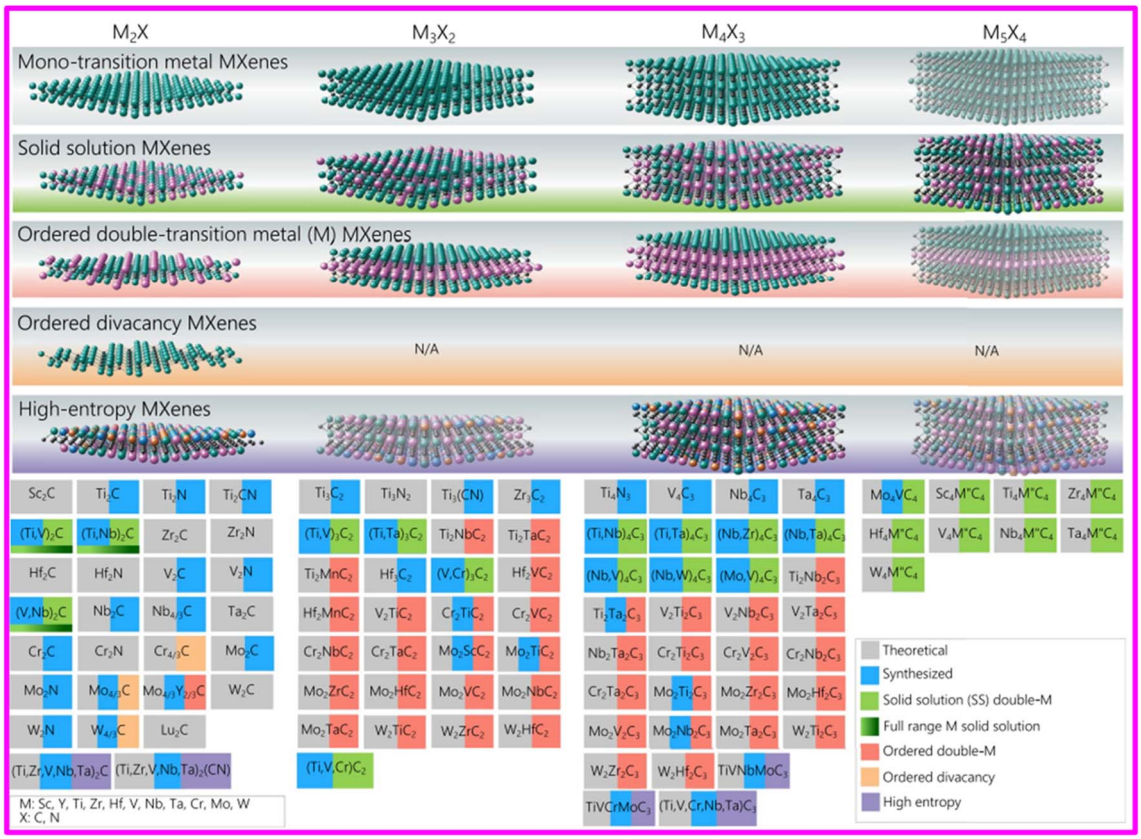

Fig. 1 MXene structures and compositions reported to date. The top row shows structures of mono-M MXenes. The second row shows solid solutions (their compositions are marked in green below). The third row shows in-plane and out-of-plane ordered double M MXenes (their compositions are marked in red). The fourth row shows an ordered divacancy structure, which has only been reported or the M_2C MXenes, making an $M_4/3C$ composition due to 1/3 of all atom positions being vacant in each M layer (their compositions are marked in orange color). The fifth row shows high-entropy MXenes (their compositions are marked in violet). This table includes both experimentally (marked in blue) and theoretically (marked in gray) explored compositions of MXenes. Surface terminations are not included. This table includes phases that are synthesized *via* bottom up or phase transformation of other phases, such as W_2N, V_2N, and Mo_2N. Reproduced with permission.[35]

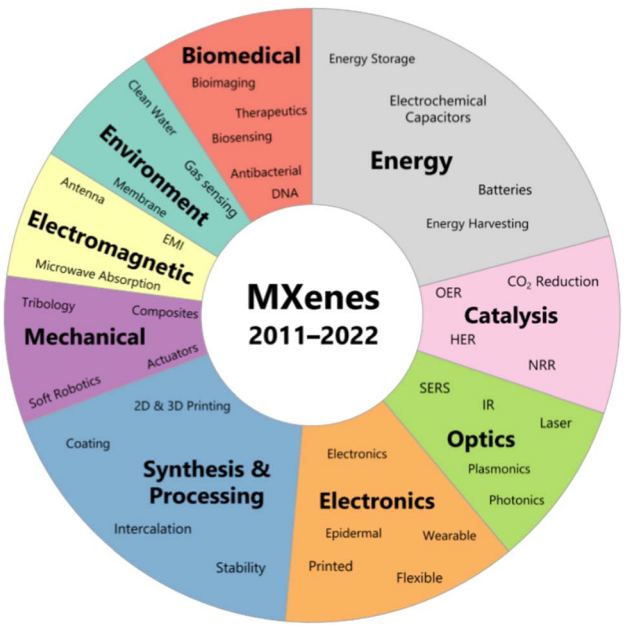

Fig. 2 Applications of MXenes in different fields. Reproduced with permission.[35]

proton exchange membranes, basic electrolysis, or solid oxide electrolysis. The hydrogen evolution reaction (HER) and oxygen evolution reaction (OER) play crucial roles in enhancing the overall efficiency of water electrolysis for energy conversion and storage. Thus, it is necessary to employ knowledge-driven principles to design optimal electrocatalysts that exhibit desirable activity, selectivity, and electrochemical stability for specific reactions.[61]

Basic mechanism of HER

The hydrogen evolution reaction (HER) holds a prominent place among the electrochemical reactions that have undergone extensive study, thanks to its relative simplicity and direct applicability in various industries, including water electrolysis. In contrast to the slow kinetics observed in the oxygen evolution reaction (OER) and oxygen reduction reaction (ORR), the HER demonstrates significantly faster kinetics when it occurs on noble metal electrodes, particularly those composed of platinum group metals (PGM). This enhanced kinetics enables the achievement of practical current densities (>1 A cm^{-2}) at just a few tens of millivolts of over potential.[58,62] The first inquiries

into understanding the mechanism of the hydrogen evolution reaction (HER) on metallic surfaces were primarily centered around nickel and took place in the early 1950s.[58] The hydrogen evolution reaction at the cathode (HER) is a twostep chemical process that involves the transfer of two electrons including the adsorption and desorption of intermediate species. The initial step of HER in acidic environment is the reduction of hydrogen by one electron followed by its adsorption at the cathode surface (H*) is termed as the Volmer step.[24,63] Following the previous step, the generation of hydrogen molecules can happen through two different paths depending on the amount of adsorbed hydrogen atoms: (i) In situations where the concentration of H* is significantly low, the H* atom acquires an electron and a proton from the water leading to the desorption of H_2 from cathode surface. This process is referred to as the 'Heyrovsky step' and the sequence is called as Volmer–Heyrovsky mechanism. And (ii), when the quantity of H* is considerably high, the generation of a hydrogen molecule occurs through the merging of two neighboring H* atoms on the surface of the cathode. This mechanism is known as the 'Tafel step' and series of steps is called Volmer–Tafel mechanism as shown in schematics of HER in acidic and alkaline conditions. The schematics of HER in acidic and alkaline conditions has been shown in Fig. 3.[58,64,65] By comparing the Tafel slope values, the predominant mechanism of the hydrogen evolution reaction (HER) for various catalysts can generally be determined. A Tafel slope $\geq$120 mV dec^{-1} indicates the deterministic Volmer reaction as the mechanism. In the range of 40–120 mV dec^{-1}, the HER is controlled by the Heyrovsky mechanism. On the other hand, a Tafel slope $\leq$40 mV dec^{-1} suggests the significant involvement of the Tafel mechanism. Based on this, it can be inferred that the HER catalytic processes of the WC@rGO and Pt–WC@rGO electrodes follow the Volmer–Heyrovsky mechanism and Volmer–Tafel mechanism, respectively.[24,66]

Basic mechanism of OER

A significant correlation has been established between the voltage required for oxygen generation on a metal surface and the redox potential of the metal/metal oxide pair as a consequence of the investigations conducted by Conway *et al.*[58] The formation of respective metal oxide is necessary for the release of oxygen from metal surface even in case of noble metals. Current studies have validated this finding, specifying that the oxygen evolution reaction (OER) primarily takes place on the hydroxide, oxyhydroxide, or oxide layer that spontaneously forms on the electrocatalyst's surface.[58,67]

The adsorbate evolution mechanism (AEM) is widely recognized as a traditional mechanism for the oxygen evolution reaction (OER). The crucial factor that determines the inherent activity of a catalyst is its ability to bind with intermediates. In electrocatalytic reactions, it is important to strike a balance in the binding strength between the active site and the intermediate.[68,69]

Unlike AEM, the lattice oxygen mechanism (LOM) involves the oxidation of the catalyst's lattice oxygen to release oxygen. Specifically, the lattice oxygen itself tends to undergo oxidation under the OER potential through lattice oxygen redox chemistry, and then participates in the OER process to generate oxygen. The LOM often surpasses the limitations of conventional AEM and provides a better explanation for the fundamental source of the remarkable catalytic activity observed in certain solid-phase catalysts. Therefore, gaining a profound understanding of the reaction mechanism and relevant parameters can serve as a guiding principle for developing more efficient OER electrocatalysts.[70] The basic mechanism of OER is shown in Fig. 4.

MXene-based hybrid architectures for HER

Hydrogen evolution reaction (HER) serves as a crucial approach for separating water and producing hydrogen. The development of HER catalysts with exceptional capabilities such as conductivity, stability, and selectivity are imperative for the establishment of a hydrogen-based economy. By reducing the excessive energy required for HER, a high-performance electrocatalyst can enhance efficiency and contribute to improved overall performance.

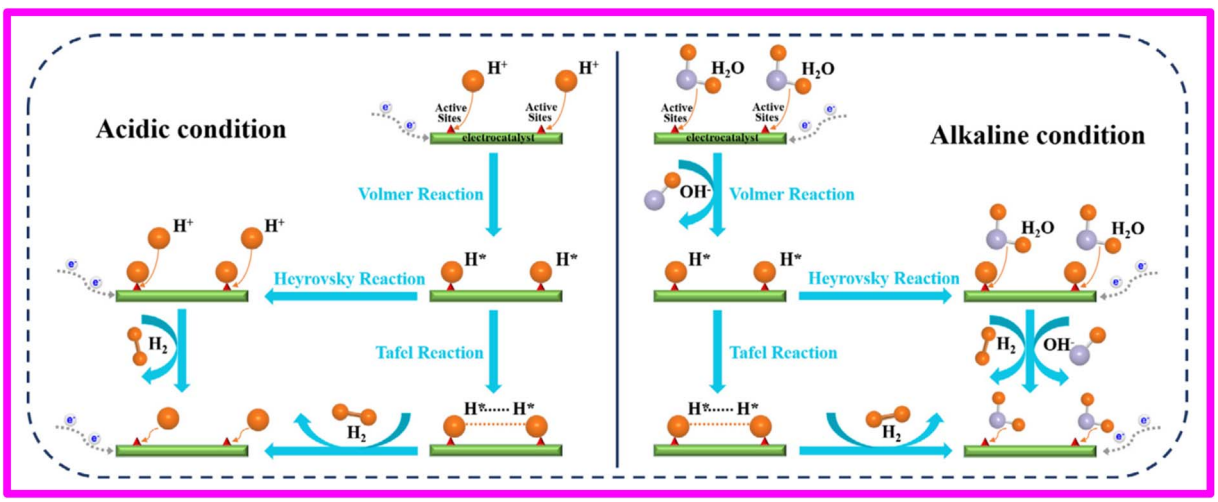

Fig. 3 Schematics of HER in acidic and alkaline conditions. Reproduced with permission.[65]

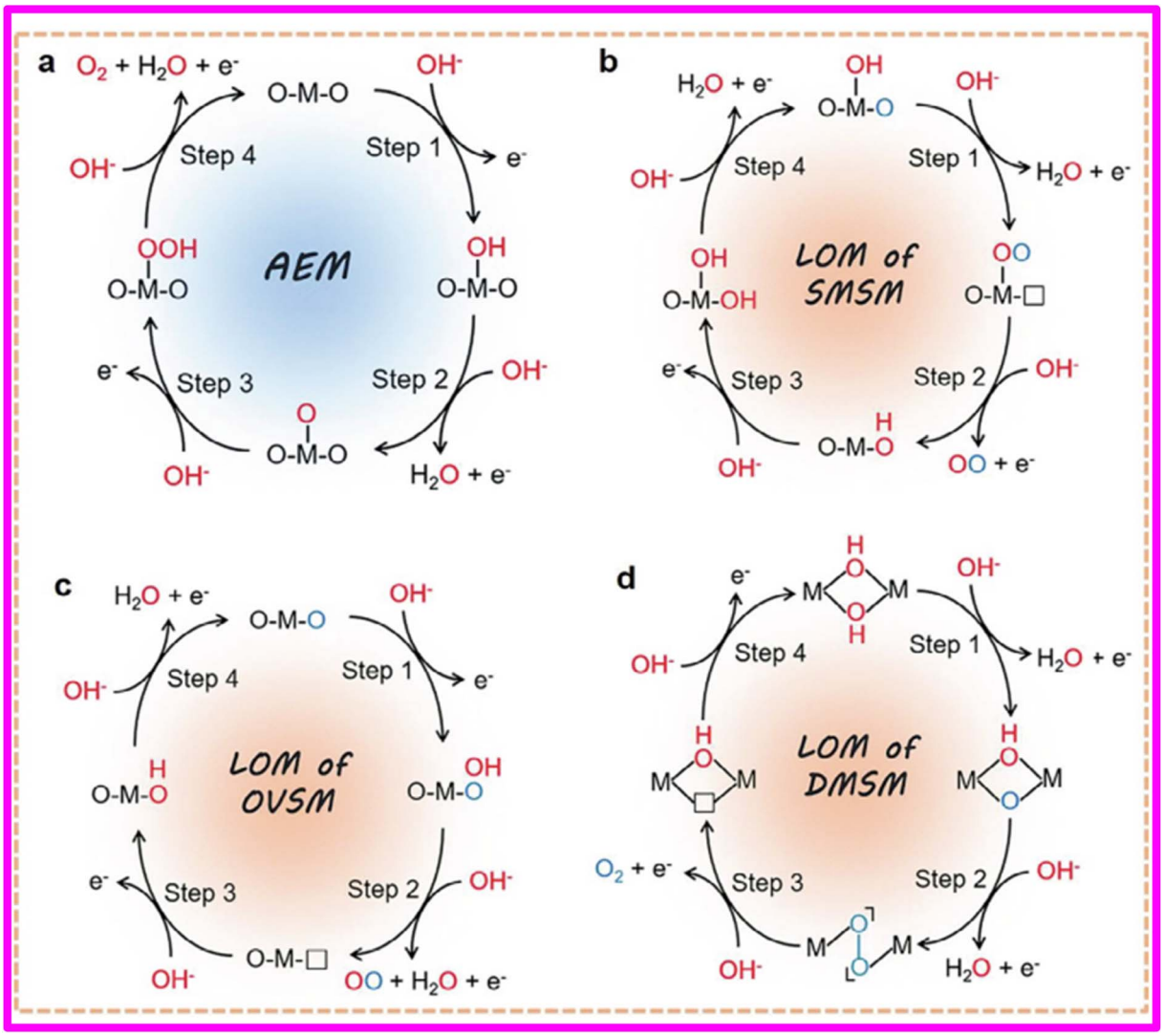

Fig. 4 Basic mechanism of OER. Reproduced with permission.[70]

While platinum (Pt)-based electrocatalysts are commonly utilized due to their excellent performance in promoting the hydrogen evolution process, their widespread commercialization has been hindered by the high cost and limited availability of metallic Pt. 2D, MXene have shown great potential as efficient electrocatalyst for hydrogen evolution reaction owing to their superb properties including very high electrical conductivity, large surface area, hydrophilicity and tunable surface chemistry.[71,72] However, long term stability and recyclability of MXenes has been limited by restacking and agglomeration of MXene flakes. The problem of restacking of MXenes can be reduced by combining it with other nano materials. The combination of metal organic frameworks (MOFs) with MXenes proves to be a successful approach due to the beneficial properties offered by MOFs, such as high surface area, porosity, diverse functionalities, pore-confinement effect, and tunable coordination space. These features create an ideal environment for hosting MXenes, preventing their agglomeration.[73] The summary of HER performance of MXene hybrid architectures has been shown in Table 1.

The electrocatalytic hydrogen evolution reaction (HER) in a mild neutral medium represents a significant objective for environmentally sustainable energy conversion. However, its progress is hindered by sluggish kinetics. Although platinum group noble metals display exceptionally high HER activities, their limited availability and performance instability constrain widespread application. Wu *et al.* demonstrated the superior HER electrocatalytic properties of highly dispersed ruthenium (Ru) clusters anchored on Mo_2CT_x MXene, leveraging the excellent catalyst carrier characteristics of 2D-layered transition metal carbides (MXenes). The Ru/Mo_2CT_x catalyst, prepared through a straightforward *in situ* reduction strategy, exhibited remarkable performance with a very low overpotential of 73 mV for achieving a current density of -10 mA cm^{-2} and a Tafel slope of 57 mV in neutral medium, surpassing performance of most previously reported MXene-based catalysts. Previous studies have established that the hydrogen evolution reaction

Table 1 Summary of HER performance of MXene hybrid architectures

Catalyst	Electrolyte	Overpotential (mV)@10 mA cm^{-2}	Tafel slope (mV dec^{-1})	Scan rate (mV s^{-1})	Ref.
Co-MoS_2/V_2C@CC	1 M KOH	70.1	98.6	10	78
CoBDC/MXene	1 M KOH	29	46	5	79
Rh-Co-Ni LDH/$Ti_3C_2T_x$	1 M KOH	74.6	43.9	5	80
LDH (60%)/MXene-RGO	1 M KOH	326	100	—	81
$Ti_3C_2T_x$: Co	1 M KOH	103.6	103.3	10	82
Ti_3CNCl_2@CoS_2	0.5 M H_2SO_4	175	89	—	72
MoS_2/Ti_3C_2@CNFs	0.5 M H_2SO_4	142	113	5	83
Pt/Nb_2CT_x-600	0.5 M H_2SO_4	5	34.6	—	84
(MIL-100)/$Ti_3C_2T_x$	0.5 M H_2SO_4	107	61	—	71
Ru/Mo_2CT_x	0.5 M H_2SO_4	64	57	5	74
Co-NCNT/$Ti_3C_2T_x$	1 M KOH	190	78	5	75
$BiFeO_3$/Cr_2CT_x	1 M KOH	128	53.3	5	76
MXene@$CoSnO_3$	1 M KOH	45	51	5	77
COF/$Ti_3C_2T_x$	0.5 M H_2SO_4	72	50	—	85
WS_2@MXene/GO	0.5 M H_2SO_4	42	45	10	86
	1 M KOH	43	58	10	

(HER) in a neutral medium involves both H_3O^+ ions (in acidic conditions) and neutral H_2O molecules (in alkaline conditions). This prediction led to the demonstration that the HER performance of Ru/Mo_2CT_x is expected to improve in both acidic and alkaline environments, as evidenced by the determined overpotentials: 64 mV at 10 mA cm^{-2} in 0.5 M H_2SO_4; and 78 mV at 10 mA cm^{-2} in 1 M KOH.

Furthermore, the Ru/Mo_2CT_x catalyst established enhanced stability when compared to commercial Pt/C. Both experimental findings and theoretical calculations suggest that the interaction among Ru clusters influences the electronic structure of active sites, facilitating the dissociation of water (H_2O) and the desorption of hydrogen.[74]

The deliberate design of transition metal catalysts exhibiting robust and enduring electrocatalytic activity for hydrogen evolution reactions (HER) holds paramount importance in the realm of renewable energy conversion, storage, and water splitting. The incorporation of heteroatoms has emerged as a viable strategy for augmenting electrocatalytic activity. Cobalt nanoparticles (Co-NPs) were enveloped by nitrogen-doped carbon nanotubes (NCNTs), fabricated through an *in situ* growth process on accordion-like $Ti_3C_2T_x$-MXene (Co-NCNT/$Ti_3C_2T_x$) in study conducted by Zhang *et al.* This unique structure showcased notable features, including abundant anchoring sites for *in situ* growth of NCNT, seamless integration of Co-NPs and NCNTs, rapid electron transfer between 1D NCNTs and 2D $Ti_3C_2T_x$-MXenes, and a substantial number of effective catalytic active sites. The Co-NCNT/$Ti_3C_2T_x$ hybrid catalyst exhibited exceptional HER performance, characterized by a low overpotential (η_{10}, 190 mV), a small Tafel slope (78.4 mV dec^{-1}), a sizable electrochemically active surface area, and robust long-term stability, surpassing the performance of numerous reported electrocatalysts. This approach presents a straightforward method for crafting transition metal HER catalysts incorporating NCNT and MXene.[75]

A versatile hierarchical composite of Bismuth ferrite/chromium carbide ($BiFeO_3$/Cr_2CT_x) MXene has been synthesized and tested as an electrocatalyst for water splitting by Reghunath and its coresearchers. In this approach, a straightforward method was proposed for synthesizing Cr_2CT_x MXene from the chromium aluminum carbide (Cr_2AlC) MAX Phase. X-ray diffraction studies, scanning electron microscopy, and high-resolution transmission electron microscopy confirmed the removal of aluminum atomic layers from the Cr_2AlC MAX structure. Electrochemical tests demonstrated that the $BiFeO_3$/Cr_2CT_x MXene composite, produced with reduced Al_2O_3 content, exhibited excellent performance in the hydrogen evolution reaction (HER) with a low overpotential of 128 mV in 1 M potassium hydroxide. Calculated values for the Tafel slope and charge transfer resistance are 53.3 mV dec^{-1} and 0.16 Ω, respectively. In a dielectrode electrolysis system, the $BiFeO_3$/Cr_2CT_x MXene electrode required only 1.81 V of cell potential to achieve 10 mA cm^{-2} with long-term stability. This study highlights the potential use of $BiFeO_3$/Cr_2CT_x MXene in HER, providing a straightforward approach for fabricating Cr_2CT_x MXene composites for HER applications.[76]

Recently, two-dimensional (2D) MXenes-based nanostructures have gained attention as effective electrocatalysts due to their remarkable electrical conductivity and superior hydrophilicity. However, their practical application in hydrogen production has been limited by low electrocatalytic activity and poor stability. This study introduces a novel approach to enhance the catalytic activity of MXene by incorporating amorphous $CoSnO_3$ onto wrinkled $Ti_3C_2T_x$ MXene nanosheets, resulting in a promising electrocatalyst (MXene@$CoSnO_3$) for the alkaline hydrogen evolution reaction (HER). The integration of $CoSnO_3$ nanocubes onto the $Ti_3C_2T_x$ MXene surface not only stabilizes MXene nanosheets against spontaneous oxidation but also establishes strong interfacial electronic coupling between the two components. This coupling facilitates electron redistribution at the MXene and $CoSnO_3$ interfaces, altering the

electronic structure around Co and enabling the activation of high-potential Sn for optimal H adsorption (ΔG_H), thereby promoting H* conversion in the HER. The MXene@$CoSnO_3$ electrocatalyst demonstrates high alkaline HER performance, exhibiting an ultralow overpotential of 45 mV at 10 mA cm^{-2}, a small Tafel slope of 51 mV dec^{-1}, and long-term stability in 1 M KOH, comparable even to commercial Pt/C catalyst.[77]

Ma *et al.* synthesized two dimensional porous nanoarchitecture from iron-based metalorganic frameworks (MIL-100) and $Ti_3C_2T_x$ MXene nanosheets (MIL/$Ti_3C_2T_x$) using an *in situ* solvothermal assembly process.[71] Fig. 5(a) represents the schematics for synthesis of MIL/$Ti_3C_2T_x$ catalyst. Fig. 5(b and c) shows the HRTEM images of MIL/$Ti_3C_2T_x$. Fig. 5(d) and (e) shows the LSV polarization curves and Tafel slopes of the Ti_3AlC_2, $Ti_3C_2T_x$ and $Ti_3C_2T_x$/MIL composites. Large number of interconnected conducting channels were created due to intercalation of MIL-100 which hindered the restacking and agglomeration of $Ti_3C_2T_x$ nanoflakes. Very good HER performance was exhibited by the composite with 40 wt% loading of the MIL in terms of low onset potential of 29 mV and small Tafel slope of 61 mV dec^{-1} along with good cyclability much better than the pristine MIL and $Ti_3C_2T_x$ catalysts. This high performance of the nanocomposite can be endowed to the formation of conducting channels and synergistic effects between MIL and $Ti_3C_2T_x$. MIL(40%)/$Ti_3C_2T_x$ showed a very much smaller value of charge transfer resistance (35.5 Ω) as compared to the pure MIL (272.9 Ω).[71]

In another work, Ma and coworkers successfully achieved the *in situ* growth of hydrazone-linked covalent organic framework (COF-42) nanocrystals exhibiting a distinctive nanoflower-shaped morphology on 2D ultrathin $Ti_3C_2T_x$ MXene nanosheets (COF/$Ti_3C_2T_x$) through a convenient and robust stereo assembly strategy. Notably, the integration of COF-42 with $Ti_3C_2T_x$ nanosheets not only created multiscale porous channels for rapid electrolyte and electron transport but also ensured the complete exposure and activation of numerous catalytically active centers. Consequently, the optimized COF/$Ti_3C_2T_x$ nanoarchitecture demonstrates outstanding hydrogen evolution reaction (HER) properties, including an exceptionally low onset potential of 19 mV, a small Tafel slope of 50 mV dec^{-1}, and reliable long-term durability, comparable to those of a commercial Pt/C catalyst. Density functional theory

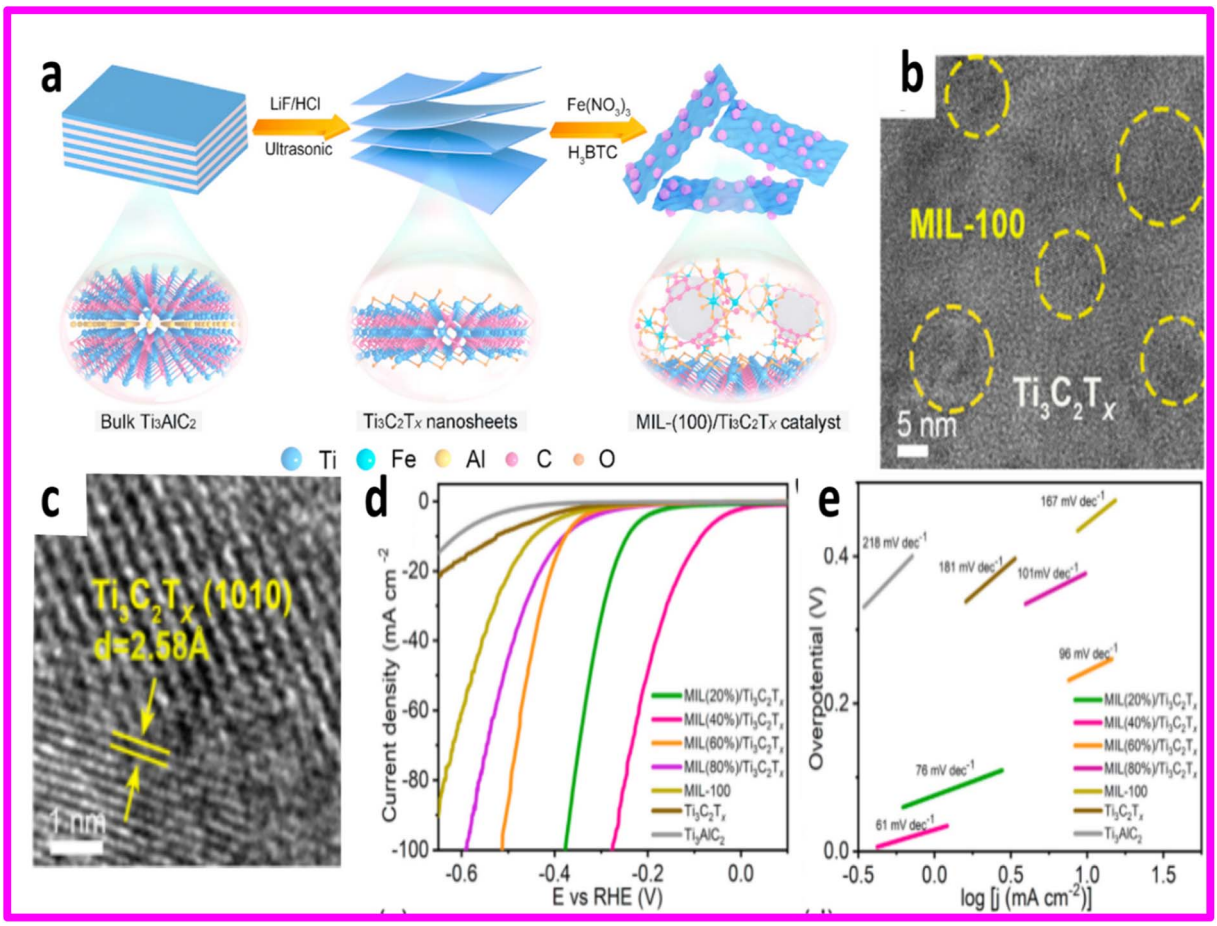

Fig. 5 (a) Schematic of the synthetic procedures for the MIL/$Ti_3C_2T_x$ catalyst, which includes preparation of $Ti_3C_2T_x$ MXene nanoflakes from bulk Ti_3AlC_2 powder; and growth of the MIL-100 nanocrystals on the surface of $Ti_3C_2T_x$ nanoflakes. (b and c) Microstructural analysis of the MIL/$Ti_3C_2T_x$ nanoarchitecture. Representative HR-TEM images of MIL/$Ti_3C_2T_x$. (d) LSV polarization curves and (e) Tafel plots of MIL/$Ti_3C_2T_x$ with diverse MIL-100 ratios, MIL-100, $Ti_3C_2T_x$, and Ti_3AlC_2 electrodes in 0.5 M H_2SO_4 solution. Reproduced with permission.[71]

calculations further revealed that the deliberate combination of COF-42 with $Ti_3C_2T_x$ provides a more diverse array of active positions with appropriate ΔG_H values, resulting in an enhanced hydrogen generation rate.[85]

In another study Wang *et al.* prepared well connected 2D/2D hybrid by coupling of MXene with CoBDC nanosheets by a facile *in situ* grown approach. The as synthesized CoBDC/MXene catalyst showed lower over potential values of 29, 41 and 76 mV in alkaline, acidic and neutral environment respectively. The main factor to attain the high HER performance was the development of interconnected Co–O–Ti bridges that facilitated the charge transfer through electronic modification of the heterostructure. Density functional theory calculations also supported the experimental observations which revealed that d-band center of cobalt (Co) in CoBDC/MXene experiences a shift towards lower energy compared to pure CoBDC. This shift suggested a weaker adsorption of hydrogen (H) intermediates on the CoBDC/MXene interface, facilitating the subsequent evolution of H_2.[79]

The unique two-dimensional (2D) lamellar structure, large surface area, and tunable chemical compositions of transition-metal-based layered double hydroxides (LDHs) have garnered significant interest among scholars. As a result, LDHs are emerging as promising nonprecious electrocatalysts.[76] Despite their potential as electrocatalysts, the practical application LDHs is hindered by several challenges. These include poor conductivity, a tendency to agglomerate, and low intrinsic activity, which impose limitations on their usability.[87] There electrocatalytic performance can be increased by combining them with MXenes. Yan and co-authors developed Rh doped Co-Ni LDH/$Ti_3C_2T_x$ nanocomposite for HER. The prepared Rh-CoNi LDH/MXene showed lower overpotential of 74.6 $\pm$ 0.4 mV at current density of 10 mA cm^{-2} and long-term stability. The electronic behavior and structure of CoNi LDH were effectively modified through Rh doping and regulated oxygen vacancies (Ov), resulting in an increased number of active sites and optimized adsorption/desorption of intermediates. Additionally, the well-constructed interface between sheets exposed a larger number of accessible active sites, thereby enhancing the electrocatalytic performance. By performing density functional theory (DFT) calculations, it was determined that the introduction of Rh and its coupling with MXene led to significant changes in the electronic structure. These modifications resulted in optimized adsorption energies for intermediates involved in the hydrogen evolution reaction (HER), consequently enhancing the intrinsic catalytic activity of CoNi LDH.[80]

In another study, Shen *et al.* devised a reliable and user-friendly approach for effectively producing a well-regulated 3D interconnected structure of Ni–Fe layered double hydroxide nanosheets (LDH) confined within a network of $Ti_3C_2T_x$ MXene-reduced graphene oxide (MX-RGO).[81] The method used was a bottom-up strategy that allows control over the synthesis process, and it employed a co-assembly technique as shown in Fig. 6(a). This integration imparted several unique benefits to the hybrid, including a significantly large specific surface area, extremely thin walls, an optimized electronic structure, a continuous structure with meso- and macropores, uniformly distributed LDH layers, and multiple channels for charge transfer. The FESEM, TEM, and HRTEM images of the LDH/MX-RGO nanoarchitecture were shown in Fig. 6(b), (c) and (d) respectively.

The authors selected five different Ni-Fe LDH mass fractions as 10%, 20%, 40%, 60%, and 80% by weight of LDH and were represented as LDH (10%)/MX-RGO, LDH (20%)/MX-RGO, LDH (40%)/MX-RGO, LDH (60%)/MX-RGO, and LDH (80%)/MX-RGO, respectively. The LDH (60%)/MX-RGO electrode unveiled the best performance for the hydrogen evolution reaction (HER) amongst different compositions tested. It displayed an onset electrode potential of only 162 mV surpassing other electrodes in terms of the rapid increase in cathodic current. Moreover, comparison of the corresponding Tafel plots revealed that the LDH (60%)/MX-RGO electrode possesses the smallest Tafel slope of 100 mV dec^{-1}. The subsequent electrodes, in increasing order of Tafel slope, are LDH (80%)/MX-RGO (131 mV dec^{-1}), LDH (40%)/MX-RGO (133 mV dec^{-1}), LDH (20%)/MX-RGO (143 mV dec^{-1}), and LDH (10%)/MX-RGO (150 mV dec^{-1}). The bare LDHs, $Ti_3C_2T_x$, RGO, Ti_3AlC_2, as well as the binary LDH/RGO and LDH/MX materials demonstrated comparatively lower HER activity and larger Tafel slopes (Fig. 6f).

The charge-transfer resistance of LDH (60%)/MX-RGO only 2.7 was significantly lower than those of LDH/MX (66.5 Ω), LDH/RGO (47.5 Ω), and bare LDHs (226.6 Ω). This finding confirms that the 3D porous $Ti_3C_2T_x$-RGO networks effectively establish numerous fast electron pathways, ensuring swift kinetics for hydrogen evolution.[81]

CoS_2 has shown promise as an electrocatalyst for the hydrogen evolution reaction (HER). Nevertheless, its widespread application is hindered by its relatively high chemisorption energy for hydrogen atoms, resulting in low HER activity. Theoretical calculations based on first-principles study disclosed that the incorporation of Cl-terminated MXenes-Ti_3CNCl_2 can effectively reduce the HER over potential of CoS_2-based materials reported by Jiang and coauthors. The value of Gibbs free energy of hydrogen adsorption ($|\Delta G_H|$) close to zero was regarded as the outcome of the formation of a core–shell nanostructure, Ti_3CNCl_2@CoS_2. Taking inspiration from the theoretical results, they successfully synthesized a distinctive core–shell nanostructure of Ti_3CNCl_2@CoS_2, by combining CoS_2 with a Cl-terminated MXenes-Ti_3CNCl_2 using facile hydrothermal method. Fig. 7(a)–(c) shows the SEM images of COS_2 nanoparticles, Ti_3CNCl_2 nano sheets and Ti_3CNCl_2@CoS_2 core shell nanostructures. The higher HER activity in 0.5 M H_2SO_4 electrolyte was evidenced by the Ti_3CNCl_2@CoS_2 in terms of small Tafel slope of 89 mV dec^{-1} and low over potential of 175 mV at 10 mA cm^{-2} in comparison with the pristine Ti_3CNCl_2 nanosheets and CoS_2 nanoparticles. This was due to synergistic effects of rapid charge transfer of highly conductive MXene nanosheets and intrinsic high catalytic activity of CoS_2 nanoparticles. The respective values of overpotential of CoS_2 and Ti_3CNCl_2 were 478 and 313 mV. The HER polarization curves and corresponding Tafel slopes have been depicted in Fig. 7(d) and (e) respectively.[72]

The use of HF etching to prepare MXene can lead to an excessive electron-accepting (eF) termination, which has the

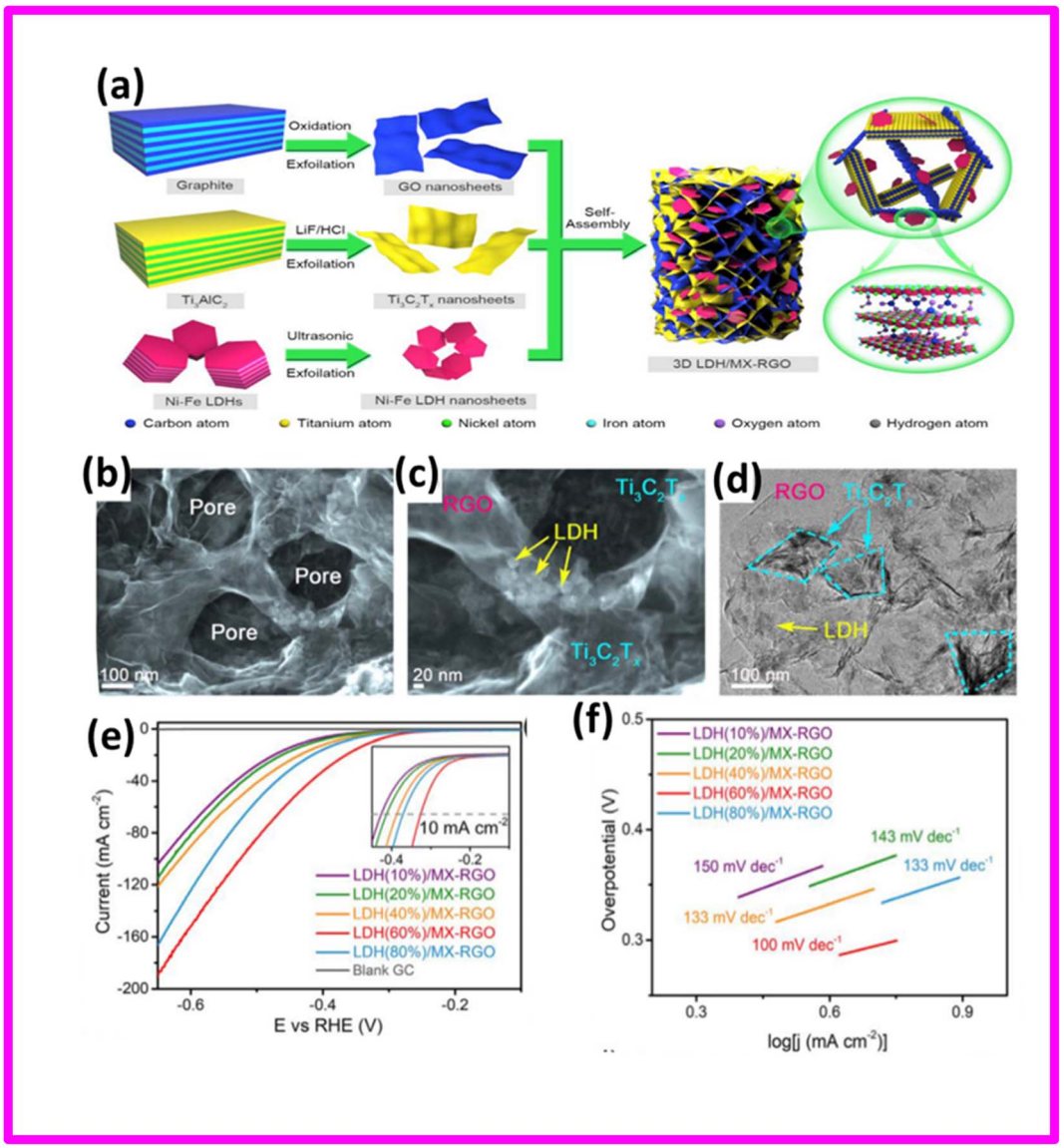

Fig. 6 (a) Schematic of the stereo assembly of the 3D LDH/MX-RGO nanoarchitecture: (1) GO was synthesized by oxidation and exfoliation of graphite; (2) $Ti_3C_2T_x$ MXene was prepared from bulk Ti_3AlC_2 MAX in the presence of LiF and HCl; (3) liquid-phase exfoliation of bulk Ni-Fe LDHs into thin Ni-Fe LDH nanolayers; (4) self-assembly of porous LDH/MX-RGO nanoarchitecture by the solvothermal reaction. (b and c). FE-SEM, TEM, and (d) HR-TEM images of the LDH/MX-RGO nanoarchitecture. (e) LSV curves and (f) Tafel plots of the LDH/MX-RGO catalysts with different LDH contents in 1 M KOH solution. Reproduced with permission.[81]

potential to negatively impact the material's electrical conductivity and electrocatalytic properties.[56] To overcome this challenge, Rong *et al.* introduced a simplified one-step etching method involving the use of $CoCl_2$ molten salt at a temperature of 750 °C to react with Ti_3AlC_2-MAX phase. This process resulted in the formation of a cobalt/titanium carbide hybrid structure denoted as $Ti_3C_2T_x$: Co. To eliminate the excessive attachment of Co atoms to the MXene surface, the hybrid structure further treated with H_2SO_4 for 12 and 24 h were named as $Ti_3C_2T_x$: Co-12 h and as $Ti_3C_2T_x$: Co-24 h respectively. Characterization studies revealed that a small number of Co atoms replaced the Al atoms within the hybrid's lattice, while the majority of Co atoms were intercalated in the interlayer space of the MXene. The HER activity of the hybrid was tested in 1.0 M KOH electrolyte. Excellent electrochemical activity was shown by the hybrid $Ti_3C_2T_x$: Co-12 h with an overpotential of 103.6 mV at current density of 10 mA cm^{-2}. The calculated values of the charge transfer resistance (R_{ct}) were determined to be 48.64 Ω, 28.65 Ω, and 42.72 Ω for the $Ti_3C_2T_x$: Co, $Ti_3C_2T_x$: Co-12 h, and $Ti_3C_2T_x$: Co-24 h samples, respectively. These values indicate that $Ti_3C_2T_x$: Co-12 h exhibited the highest electrical conductivity among the tested samples. Based on this data, the surface-specific double-layer capacitance (C_{dl}) was estimated for each sample. $Ti_3C_2T_x$: Co-12 h showed the highest C_{dl} value of 18.78 mF cm^{-2}, surpassing $Ti_3C_2T_x$: Co (9.96 mF cm^{-2}) and $Ti_3C_2T_x$: Co-24 h (15.09 mF cm^{-2}). These measurements confirm that $Ti_3C_2T_x$: Co-12 h possessed a significantly larger electroactive surface area (ECSA) compared to the other samples, providing

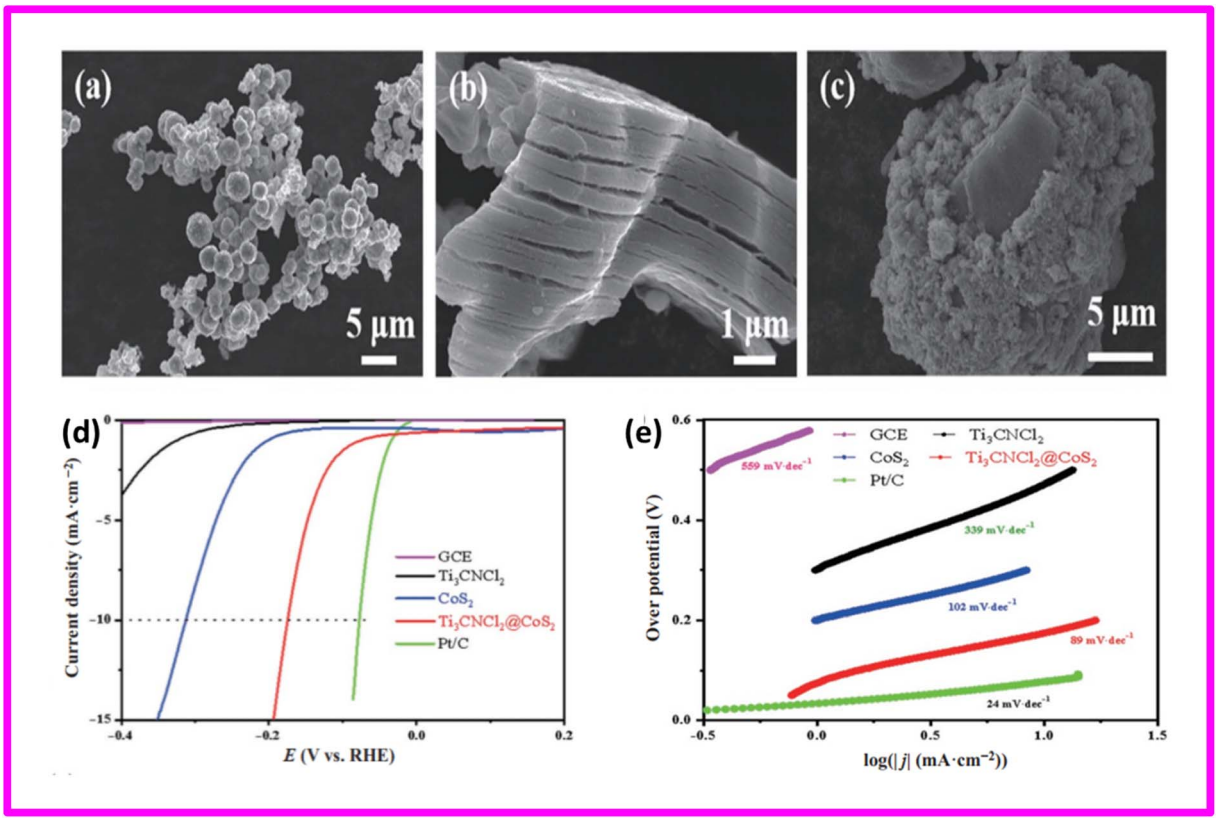

Fig. 7 SEM images of (a) CoS_2 microspheres (b) Ti_3CNCl_2 nanosheets (c) Ti_3CNCl_2@CoS_2 core shell nanostructures (d) polarization curves (e) corresponding Tafel slopes. Reproduced with permission.[72]

more catalytically active sites for the process of HER (hydrogen evolution reaction). Additionally, the results suggest that prolonged acid etching time can disrupt the two-dimensional layered structure, resulting in a decrease in the number of active sites.[82]

The two-dimensional transition metal dichalcogenides (TMDs) have shown great performance in hydrogen evolution reaction owing to their catalytically active edge sites and low Gibbs free energy for hydrogen absorption (ΔG_{H^*}) meanwhile retaining the inert nature of their basal planes. Hussain *et al.* developed interconnected porous WS2 nanosheets within MXene/GO matrices (WS_2@MXene/GO) using a straightforward hydrothermal method for applications in electrochemical supercapacitors and water splitting reactions. The WS2@MXene/GO nanocomposites, as electrocatalysts, displayed low overpotentials of 42 mV and 45 mV, along with small Tafel slope values of 43 mV dec^{-1} and 58 mV dec^{-1} for the hydrogen evolution reaction in acidic and alkaline media, respectively. Additionally, density functional theory (DFT) approximations substantiated the observed experimental outcomes through calculations of density of states, Gibbs free energy for H-adsorption, and quantum capacitance.[86]

A renowned member of the transition metal dichalcogenides (TMDCs) family is molybdenum disulfide (MoS_2) with its hexagonal structure and a sandwich-like configuration of sulfur and molybdenum atoms. The remarkable reactivity and catalytic performance displayed by MoS_2 nanoparticles have expanded its potential for various applications. Moreover, MoS_2 offers several advantages, including a hydrogen release Gibbs free energy comparable to platinum, a significant presence of active edge sites and a large specific surface area.[83] Ma *et al.* synthesized a highly efficient and stable HER electrocatalyst comprising of MoS_2, Ti_3C_2 and CNFs (carbon nanofibers) (schematics shown in Fig. 8(a)). In the first step plane-line like skeleton structure was constructed from Ti_3C_2 and CNFs which assisted to prevent restacking of MXene flakes. Then the spontaneous growth of MoS_2 on the fiber skeleton was carried out to attain a stereo structured MoS_2/Ti_3C_2@CNFs. SEM images of MoS_2/Ti_3C_2@CNFs in different magnification: (b) 12 000×; (c) 18 000× were shown in Fig. 8(b) and (c) respectively. This unique structure resulted in more extensible layered structure and significant improvement in electrical conductivity. The HER polarization curves for MoS_2, MoS_2/Ti_3C_2@-CNFs, MoS_2/Ti_3C_2, and Ti_3C_2@CNFs catalysts in a 0.5 M H_2SO_4 electrolyte were shown in Fig. 8(d). The catalytic performance of commercial Pt/C was also investigated for comparison. The MoS_2/Ti_3C_2@CNFs catalyst revealed a significantly lower overpotential of 142 mV *vs.* RHE at a HER current of 10 mA cm^{-2} (η_{10}) compared to 471 mV for MoS_2/Ti_3C_2 and 596 mV for MoS_2 alone. This indicates that the fiber skeleton structure of MoS_2/Ti_3C_2@CNFs greatly improved the catalytic performance of the HER, signifying that CNFs effectively provided a stable framework for the catalyst, allowing effective loading of MoS_2 and showcasing excellent HER activity.

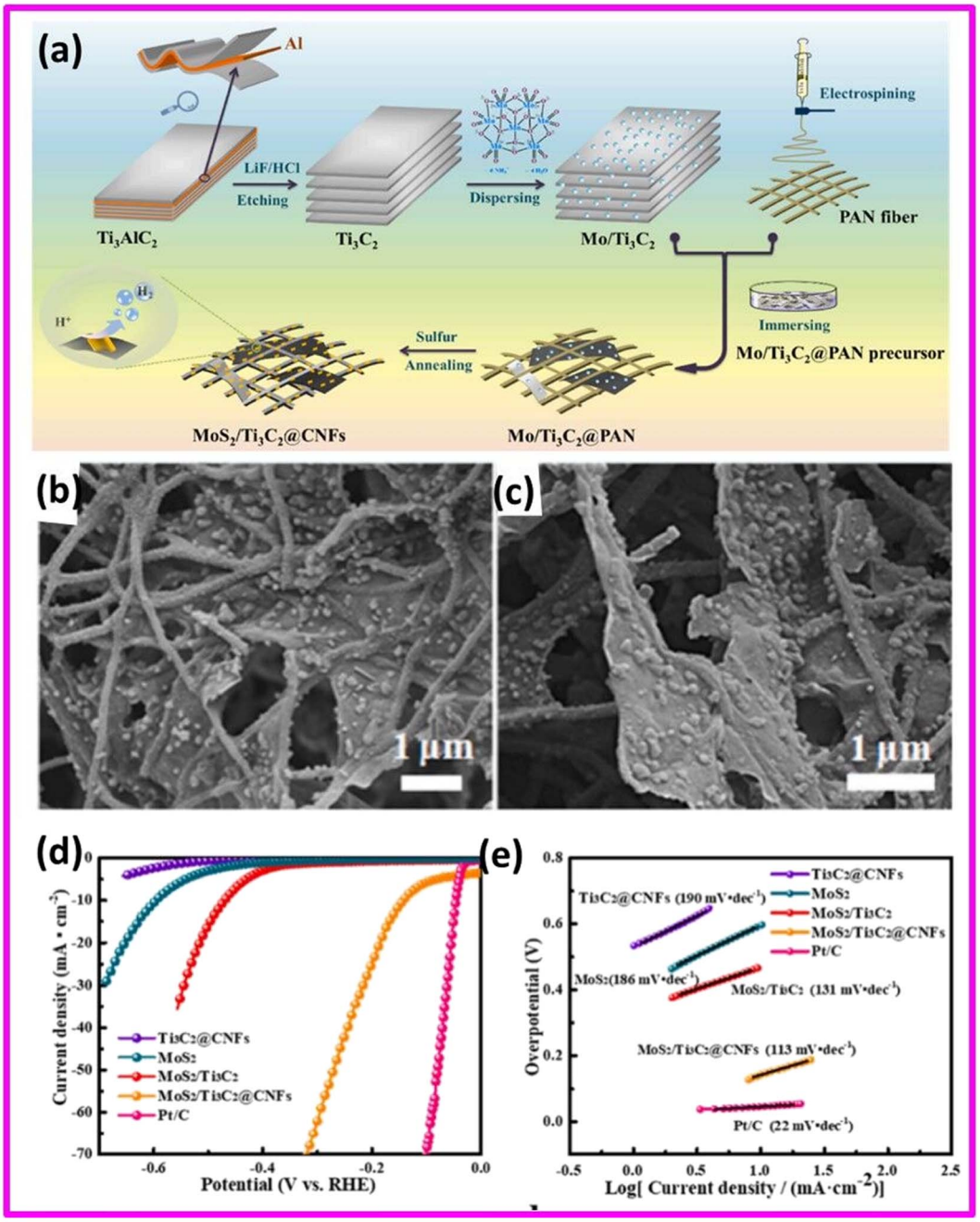

Fig. 8 (a) Synthetic schematic of MoS_2/Ti_3C_2@CNFs. SEM images of MoS_2/Ti_3C_2@CNFs in different magnification: (b) 12 000×; (c) 18 000× (d) polarization curves of MoS_2, MoS_2/Ti_3C_2, Ti_3C_2@CNFs, MoS_2/Ti_3C_2@CNFs and Pt/C catalysts at a scanning rate of 10 mV s^{-1} in 0.5 M H_2SO_4; (e) Tafel plots of several catalysts. Reproduced with permission.[83]

The Tafel slope of the MoS_2/Ti_3C_2@CNFs catalyst was measured to be 113 mV dec^{-1}, which was lower compared to MoS_2, MoS_2/Ti_3C_2, and Ti_3C_2@CNFs. This reduction in the Tafel slope of MoS_2/Ti_3C_2@CNFs was also attributed to the construction of the fiber skeleton structure, which likely changed the rate-determining step and enhanced the reaction kinetics of the catalyst. Additionally, the MoS_2/Ti_3C_2@CNFs catalyst followed the Volmer–Heyrovsky mechanism Fig. 8(f).[83]

In another study, Fan *et al.* presented a straightforward approach utilizing mechanochemical ball milling and annealing to synthesize Pt_3Nb alloy nanoclusters immobilized on the Nb_2CT_x substrate at a large scale. The application of mechanical force and the slow chemical kinetics during the process facilitated the reduction and even distribution of Pt species, enabling the efficient production of noble metal catalysts supported on the substrate. Furthermore, the subsequent thermal treatment under an argon atmosphere enhanced the interaction between the Pt nanoclusters and Nb_2CT_x substrates, resulting in the formation of the Pt_3Nb alloy.

The as-synthesized catalyst Pt/Nb_2CT_x-600, exhibited outstanding electrochemical HER performance and stability in 0.5 M H_2SO_4 electrolyte. It achieved significantly lower overpotentials of 5 mV and 46 mV, respectively, to drive current densities of 10 mA cm^{-2} and 100 mA cm^{-2} and Tafel slope of 34.66 mV dec^{-1}. This performance outshined that of other catalysts based on Nb_2CT_x and even commercial Pt/C catalysts. Accelerated durability tests (ADTs) and long-term chronoamperometry (CA) tests confirmed long term durability of the electrocatalyst. The outstanding performance in the hydrogen evolution reaction (HER) was ascribed to the effective dispersion of Pt and increased exposure of active sites achieved through the mechanochemical process and subsequent thermal treatment.[84]

Among the various types of MXenes, V-based MXenes have been identified as a potential conductive substrate within the family. These MXenes contain multiple oxidation states of the V ion on their surface layers, which boosts charge transfer between the adsorbate and the MXenes support. However, there is a paucity of theoretical and experimental studies on V-based MXenes as compared to Ti-based and Mo-based MXenes. Their development and application in hybrid systems for the hydrogen evolution reaction (HER) are still in their early stages. Therefore, further research into V_2C-based synergistic hybrid systems is essential and needs more focus for electrochemical applications.

A method of interfacial engineering was adopted by Chen *et al.* to develop a hybrid material comprising Co-doped 1T-MoS_2 coupled with V_2C MXene, which effectively improved the kinetics of the hydrogen evolution reaction (HER) in MoS_2. The smaller overpotentials values of 70.1, 263.2 and 296 mV to reach current densities of 10, 500 and 1000 mA cm^{-2} respectively, indicated excellent HER performance of the Co-MoS_2/V_2C@CC nanohybrid along with an outstanding HER stability for 50 h without degradation.

It was observed that both the pure carbon cloth (CC) and the pristine V_2C@CC presented lower catalytic activity. Owing to this MoS_2 was evaluated as the active phase responsible for the hydrogen evolution reaction (HER).

The $CoMoS_2/V_2C$@CC catalyst demonstrated the lowest Tafel slope of 98.6 mV dec^{-1} compared to Co-MoS_2@CC (109.7 mV dec^{-1}), MoS_2/V_2C@CC (127.4 mV dec^{-1}), and V_2C@CC (163.1 mV dec^{-1}), indicating its superior hydrogen evolution reaction (HER) rate and faster kinetics. The Tafel slope value of 98.6 mV dec^{-1} suggested a Volmer–Heyrovsky mechanism during HER, with the Heyrovsky step ($H_{ads} + H_3O^+ + e^- \leftrightharpoons H_2 + H_2O$) as the rate-determining step. The improved Tafel slope of Co-MoS_2/V_2C@CC compared to Co-MoS_2@CC and MoS_2/V_2C@CC confirmed that the introduction of Co doping and coupling V_2C MXene with MoS_2 efficiently facilitated dissociation of water in the Volmer step, leading to faster HER kinetics and improved intrinsic activity, in agreement with DFT calculation results. The electrochemically active surface area (ECSA) was calculated based on the electrochemical double-layer capacitance (C_{dl}) measurements, indicating that the Co-MoS_2/V_2C@CC sample exhibits the largest C_{dl} value of 25.8 mF cm^{-2} among the Co-MoS_2@CC (19.2 mF cm^{-2}), MoS_2/V_2C@CC (12.9 mF cm^{-2}), and V_2C@CC (2.9 mF cm^{-2}) samples. Consequently, the Co-MoS_2/V_2C@CC catalyst also possesses the highest ECSA among the synthesized catalysts, with a calculated value of 645 cm^2.[78] A graphical comparison of HER performance of different hybrid architectures of MXenes is shown in Fig. 9.

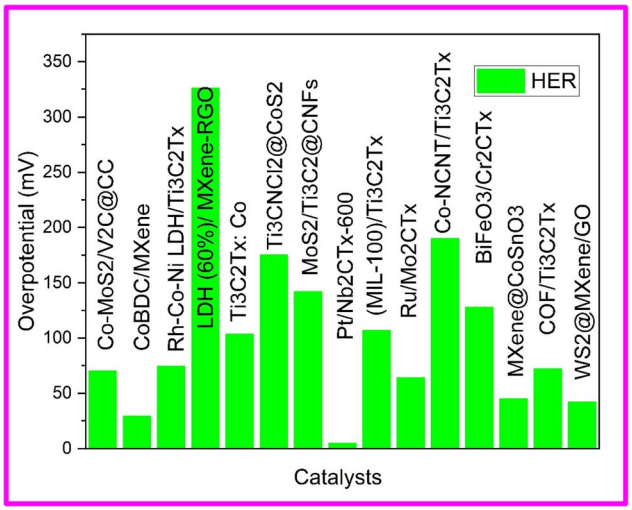

Fig. 9 A graphical comparison of HER performance of different hybrid architectures of MXenes.

Wen *et al.* explored the electrocatalytic water splitting potential of double transition metal MXene $TiVCT_x$ by developing a conductive electrode based on creating a hybrid material ($TiVCT_x$@NF) *via* deposition of 2D $TiVCT_x$ nanosheets onto a 3D network-structured nickel foam (NF). $TiVCT_x$@NF demonstrated effective electrochemical properties, displaying a low overpotential of 151 mV at 10 mA cm^{-2} and a small Tafel slope of 116 mV dec^{-1}. The open layer structure and robust interfacial coupling effect contribute to a substantial increase in active sites for the hydrogen evolution reaction (HER) and reduced resistance for charge transfer compared to the original structure. Additionally, $TiVCT_x$@NF exhibited enhanced stability in long-term acidic electrolytes.[78]

MXene-based hybrid architectures for OER

When comparing the hydrogen evolution reaction (HER) to the oxygen evolution reaction (OER), it is evident that the OER is a more intricate process. It involves a four-electron transfer mechanism and the formation of various intermediate products. To achieve effective and long-lasting OER performance, electrocatalysts with complex heterostructure and design are often necessary. While bare MXenes themselves are not efficient catalysts for OER, they can be utilized as electrically conductive supports. They can also modify the electronic properties of the coupled OER catalyst and even introduce additional active sites for OER, resulting in a significant enhancement of OER activity.[28]

Du *et al.* explored the OER performance of *in situ* grown cobalt-nickel bimetallic MOF nanosheets on $Ti_3C_2T_x$ MXene. Contrary to earlier reports they witnessed a passive effect of MXene on OER activity CoNi-MOFNs along with the

improvement in electrical conductivity of the nanocomposite. The formation of active species for OER were suppressed by unfavorable transfer of electrons from MXene to CoNi-MOFNs was held responsible for reduction in OER performance of the nanocomposite CoNi-MOFNs@MX. Individually, Co-MOFNs and Ni-MOFNs demonstrated larger Tafel slopes of 86.5 mV dec^{-1} and 196.3 mV dec^{-1} respectively as compared to CoNi-MOFNs composites. The increased reaction kinetics due to electronic coupling between Ni and Co might be the reason for much lower Tafel slopes of CoNi-MOFNs composites. Furthermore, the coupling of $Ti_3C_2T_x$ with CoNi40-MOFs leads to the disappearance of Ni^{2+}/Ni^{3+} peaks in the Tafel slope, indicating the cessation of electronic transitions from Ni^{2+} and the establishment of a strong interfacial coupling between $Ti_3C_2T_x$ and the electrocatalytic species. This phenomenon can be attributed to the presence of surface terminal groups on $Ti_3C_2T_x$, which promote the efficient interaction and integration of the two materials.[88] The summary of OER performance of MXene hybrid architectures has been shown in Table 2.

Chen *et al.* used hydrothermal method for *in situ* assembling of V_2C and hypophosphite intercalated FeNi-LDH nanosheets (H_2PO_2-/FeNi-LDH-V_2C) to boost its OER performance. In 1.0 M KOH electrolyte, the H_2PO_2-/FeNiLDH-V_2C composite demonstrated impressive electrocatalytic activity in the oxygen evolution reaction (OER). It achieved an over potential of 250 mV (η_{10}) and exhibits a small Tafel slope of 46.5 mV dec^{-1}. The remarkable OER performance and structural stability of the composite were attributed to the strong interaction and electronic coupling between FeNi-LDHs and V_2C MXene. This interaction eased significant charge transfer between the two components, resulting in an optimal adsorption/desorption balance for the OER reaction pathway. The reduction in the oxygen (O) adsorption capacity was witnessed by downward shifting the d-band center of Fe/Ni atoms. This shift created a suitable equilibrium between the adsorption of hydroxyl (OH) species and the desorption of oxygen gas (O_2). Ultimately, these factors contribute to the enhanced intrinsic activity of the composite.[89]

Hao *et al.* synthesized a hybrid catalyst for the oxygen evolution reaction (OER) by depositing CoFe-LDH (layered double hydroxide) onto the surface of Ti_3C_2 MXene nanosheets (Schematics shown in Fig. 9(a)). The resulting catalyst demonstrated higher OER activity compared to the widely used RuO_2 catalyst. The enhanced OER performance was endowed to the combined oxygen-breaking ability of CoFe-LDH and the ultra-high electrical conductivity of the Ti_3C_2 MXene substrate. Moreover, the direct growth of CoFe-LDH on the hydroxyl-rich surface of MXene well prevented aggregation of flakes, leading to increased exposure of active sites at the edges of CoFe-LDH. The interface between CoFe-LDH and Ti_3C_2 MXene eased efficient charge transfer and oxygen activation, as supported by density functional theory calculation results. Remarkably, the direct growth of CoFe-LDH on MXene imparted metallic features to the initially insulating LDH, with the O 2p states distributed above the Fermi level, which may be mediated by an anionic redox process. The LSV and Tafel plots of CoFe-LDH/MXene nanohybrid were shown in Fig. 10g and h respectively.

The LDH–MXene hybrid exhibited exceptional electrocatalytic performance. It achieved an overpotential of 319 mV at a current density of 10 mA cm^{-2} and a Tafel slope of 50 mV dec^{-1}. These results indicate a significant improvement compared to the performance of the pristine LDH, a physical mixture of LDH with MXene, and hybrids of CoFe-LDH grown on other conductive supports. The exceptional electrochemical performance of the CoFe-LDH/MXene hybrid for OER can be attributed to the array-like structure of CoFe-LDH/MXene which prevented aggregation of LDH sheets, resulting in maximum exposure of edge active sites and intimate contact with electrolytes. Moreover, the high conductivity of the MXene substrate eliminated limitations imposed by the charge transfer process.[90]

Owing to their modifiable structure and composition, Prussian blue analogues (PBAs) and their derivatives have extended significant consideration for various applications, particularly in the oxygen evolution reaction (OER). Zhu *et al.* used an *in situ* coprecipitation and subsequent phosphorization process to develop FeP-CoP nanocubes from PBAs and dispersed them on $Ti_3C_2T_x$ MXene (schematics shown in Fig. 11g). A reduction in the size of FeP-CoP nanocubes was observed was observed due to the presence of $Ti_3C_2T_x$ MXene leading to an increase in the number of active sites. Additionally, the strong coupling interaction between FeP-CoP and $Ti_3C_2T_x$ MXene enhanced the intrinsic activities of the catalyst and facilitated faster charge transfer kinetics. As a result, the optimized FeP-CoP/$Ti_3C_2T_x$-5 catalyst exhibited a low overpotential of 270 mV to drive a current density of 10 mA cm^{-2} and a small Tafel slope of 49.1 mV dec^{-1} in a 1.0 M KOH electrolyte. Fig. 11(a–f) shows SEM and TEM images of all samples.

Table 2 Summary of OER performance of MXene hybrid architectures

Catalyst	Electrolyte	Overpotential (mV)@10 mA cm^{-2}	Tafel slope (mV dec^{-1})	Scan rate (mV s^{-1})	Ref.
$CoNi_{20}$MOFNs@Ti_3C_2	1 M KOH	394	61.6	1	88
H_2PO_2-/FeNiLDH-V_2C	1 M KOH	250	46.5	5	89
CoFe-LDH/ Ti_3C_2	1 M KOH	319	50	5	90
FeP-CoP/$Ti_3C_2T_x$-5	1 M KOH	270	49.1	5	91
CDs@(PdFeNiCo)Nb_x	1 M KOH	240	62	10	92
NiCo-LDH/$Ti_3C_2T_x$/NF	1 M KOH	223	47.2	5	93
Ti3C1.8N0.2	1 M KOH	245.8	216.4	5	94
$Mo_2TiC_2T_x$ (R_{AL}-M)	0.5 M H_2SO_4	222	50.4	2	95

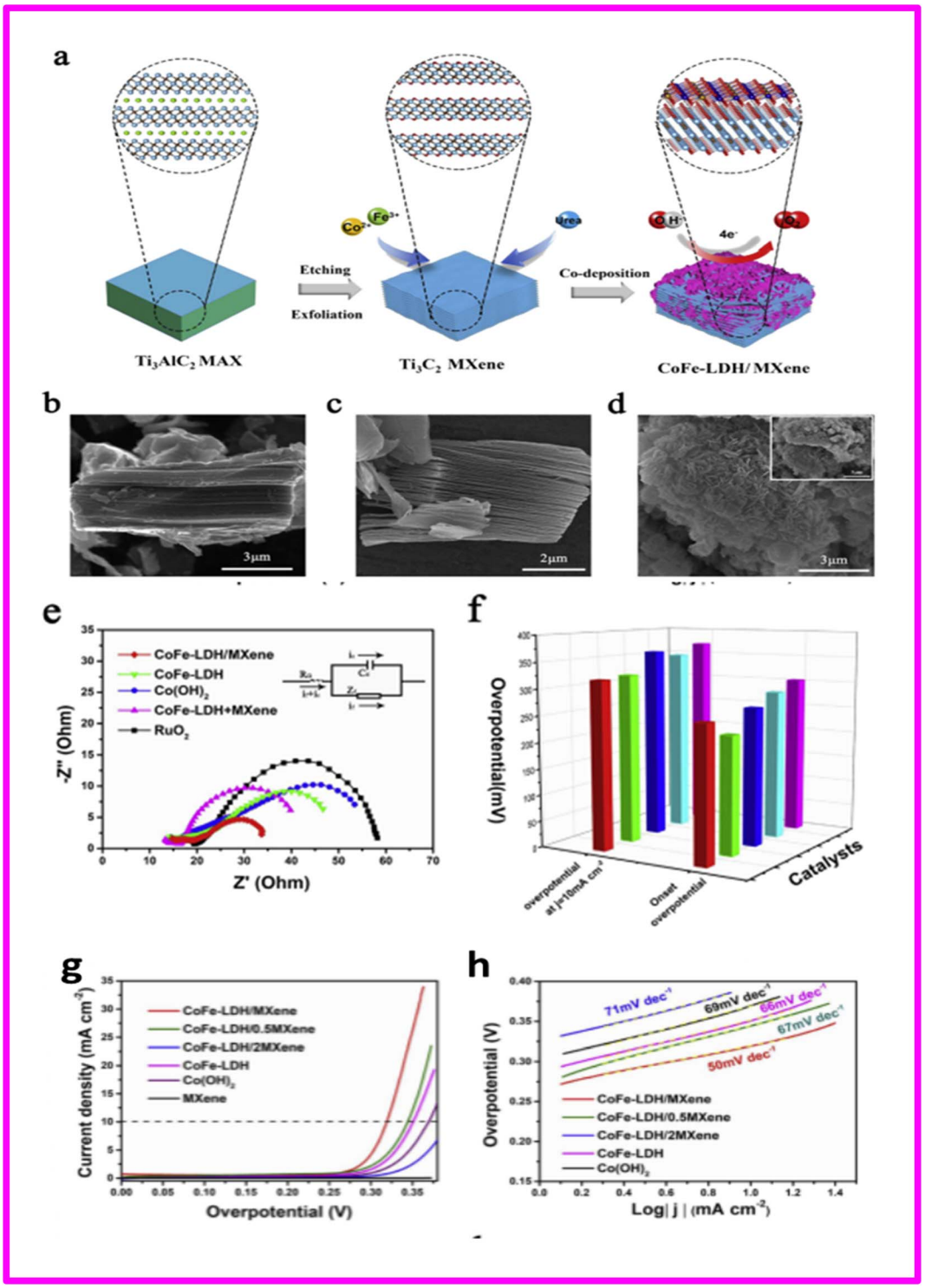

Fig. 10 (a) Scheme illustration of the formation process of CoFe-LDH/MXene hybrids. SEM images of (b) MAX (c) MXene and (d) CoFe-LDH/MXene nanohybrids. (e) EIS curves of CoFe-LDH/MXene nanohybrid, pristine LDH, physical mixture of LDH and MXene and commercial RuO_2. (f) Onset potential and overpotential at current density of 10 mA cm^{-2} for a series of catalysts (columns from left to right are red for CoFe-LDH/MXene, green for RuO_2, blue for CoFe-LDH/MXene, light blue for CoFe-LDH and magenta for $Co(OH)_2$). (g and h) The LSV and Tafel plots of CoFe-LDH/MXene nanohybrid with different mass ratio, pristine LDH, pristine $Co(OH)_2$, pristine MXene, physical mixture of LDH and MXene and commercial RuO_2. Reproduced with permission.[90]

The FeP-CoP/$Ti_3C_2T_x$ composite demonstrates improved electrochemical performance for the oxygen evolution reaction (OER) in alkaline media, exhibiting lower overpotential and a smaller Tafel slope compared to the pure phosphide counterpart. Furthermore, the composite outclassed commercial RuO_2 and several other phosphides derived from Prussian blue

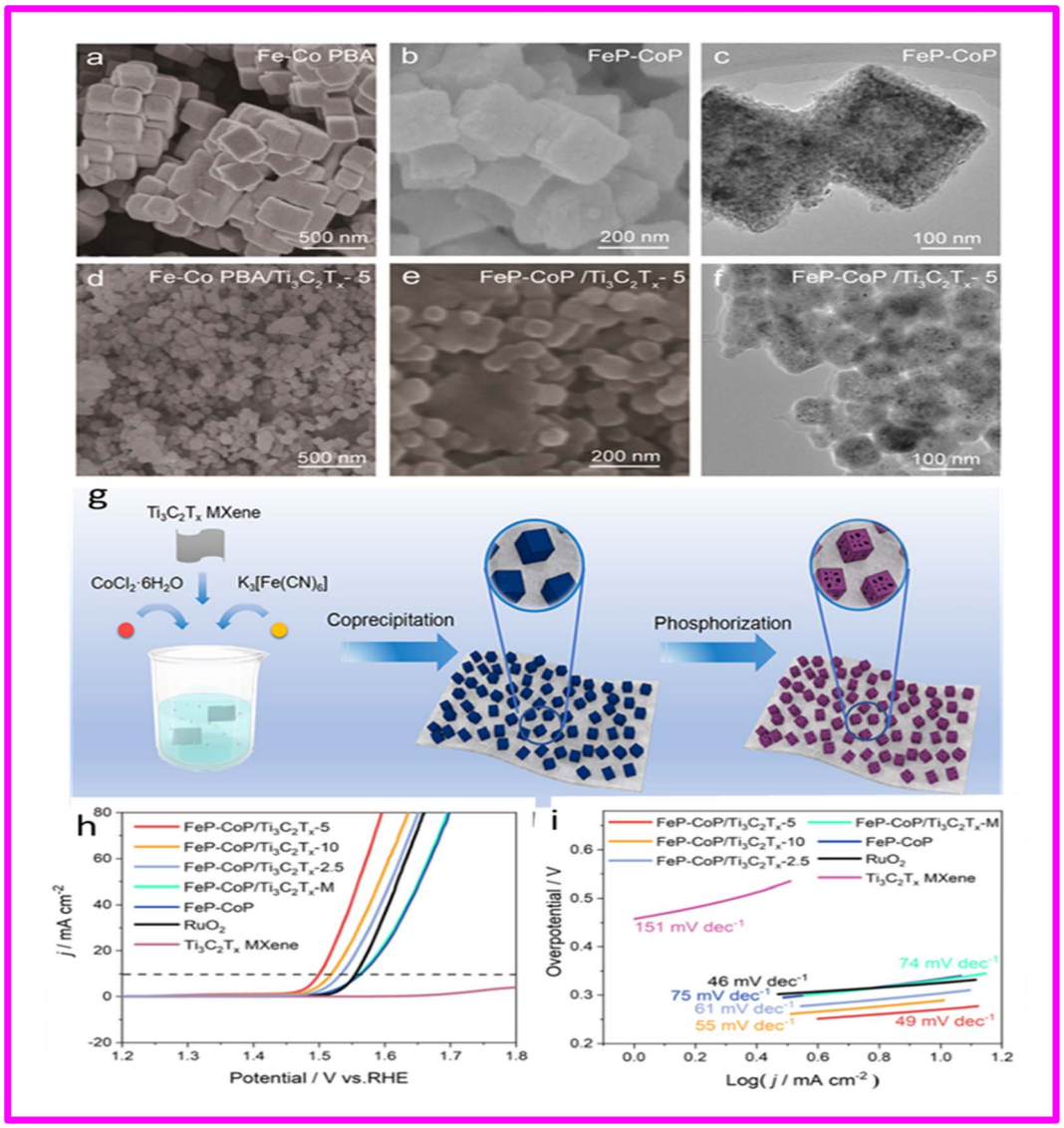

Fig. 11 (a) SEM image of Fe-Co PBA; (b) SEM image of FeP-CoP; (c) TEM image of FeP-CoP; (d) SEM image of Fe-Co PBA/$Ti_3C_2T_x$-5; (e) SEM image of FeP-CoP/$Ti_3C_2T_x$-5; (f) TEM image of FeP-CoP/$Ti_3C_2T_x$-5; (g) Scheme 1. Illustration of the Preparation of the FeP-CoP/$Ti_3C_2T_x$-*y* electrocatalysts (h) polarization curves (without iR correction) of FeP-CoP/$Ti_3C_2T_x$-*y* and control samples for the OER in 1.0 M KOH; (i) corresponding Tafel plots of FeP-CoP/$Ti_3C_2T_x$-*y* and control samples. Reproduced with permission.[91]

analogues (PBAs). The enhanced performance of the FeP-CoP/$Ti_3C_2T_x$ composite was ascribed to the presence of more active sites, higher intrinsic activity, and faster charge transfer kinetics facilitated by the introduction of $Ti_3C_2T_x$ MXene.[91]

Yan *et al.* synthesized novel electrocatalyst for OER by mixing niobium carbide quantum dots (Nb2C QDs) with various metal alloys *via* a practical solution-phase (SP) method. This method produced diverse metal alloys, including $NbPd_3$, FeNb, $NbNi_3$, $CoNbO_4$, and PdNPs, through the reduction of transition metal and palladium ions. The prepared electrocatalyst comprising uniformly dispersed CD nanoparticles integrated with (PdFeNiCo) metal alloys and Nb_2C QDs, demonstrated outstanding stability in an aqueous solution. Furthermore, owing to the superior electrocatalytic properties of these metal alloys and Nb_2C QDs, this hybrid electrocatalyst, CDs@(PdFeNiCo)Nb_x, exhibited enhanced OER performance compared to samples that were physically mixed. It achieved a low overpotential of 240 mV at a current density of 10 mA cm^{-2} and small Tafel slope of 62 mV dec^{-1}.[92] Fig. 12A graphical comparison of OER performance of different hybrid architectures of MXenes.

In another study, a three-dimensional flower-shaped layered double hydroxide (NiCo-LDH) was synthesized by Li *et al.* on titanium carbide MXene ($Ti_3C_2T_x$) coated nickel foam to form a NiCo-LDH/$Ti_3C_2T_x$/NF hybrid electrocatalyst, aimed at enhancing the oxygen evolution reaction (OER) performance. The findings demonstrated that the hybrid electrocatalyst exhibited outstanding OER activity in an alkaline solution, achieving a low overpotential of 223 mV and a small Tafel slope of 47.2 mV dec^{-1} at a current density of 100 mA cm^{-2}. The interaction at the interface and efficient charge transfer

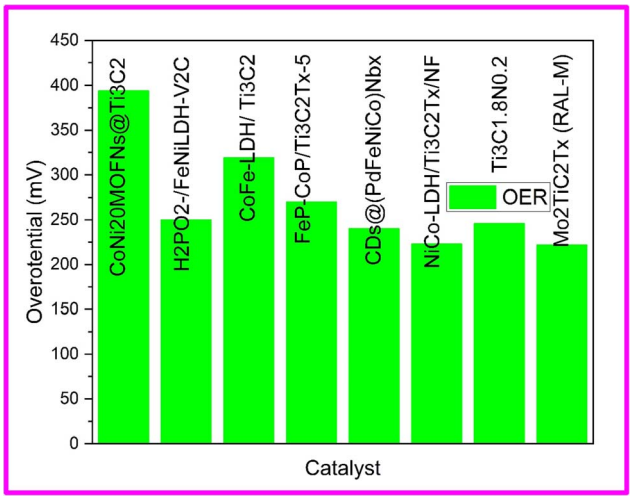

Fig. 12 A graphical comparison of OER performance of different hybrid architectures of MXenes.

between $Ti_3C_2T_x$ and NiCo-LDH contributed to an accelerated electron transfer rate during the redox process, thereby improving the overall catalytic activity of the reaction.[93]

Various researchers have enhanced the electrocatalytic performance of bare MXenes by incorporating nitrogen, thereby improving both metallic conductivity and the exposure of active sites. Recently, Tang *et al.* employed an *in situ* solution method followed by an etching route to produce nanosheets of N-doped few-layered Ti_3C_2 with varying concentrations of nitrogen content ($Ti_3C1.8N_{0.2}$ and $Ti_3C_{1.6}N_{0.4}$). The incorporation of nitrogen on the $Ti_3C_{1.6}N_{0.4}$ flakes was found to expose more active sites, facilitating a faster electron charge transfer rate and improving wettability. Consequently, the $Ti_3C_{1.6}$-$N_{0.4}$ catalyst demonstrated superior oxygen evolution reaction (OER) performance, characterized by a significantly reduced overpotential of 245.8 mV and a small Tafel value of 216.4 mV dec^{-1}. In contrast, the bare Ti_3C_2 and $Ti_3C_{1.8}N_{0.2}$ exhibited higher overpotentials of 449.0 and 418.7, respectively. Additionally, the N-doped MXenes of $Ti_3C_2T_x$-N_6 exhibited a low OER overpotential of 0.51 V and 0.36 V to achieve current densities of 100 mA cm^{-2} and 10 mA cm^{-2}, respectively. The $Ti_3C_2T_x$-N_6 catalyst also demonstrated a small Tafel value of 76.68 mV dec^{-1}, indicating the fastest OER reaction kinetics attributed to nitrogen doping.[94,96]

Advancements in acidic water splitting have been constrained due to low oxygen evolution reaction (OER) activities, sluggish reaction kinetics, and substantial catalyst degradation. Consequently, there is a critical need for a highly active and durable OER catalyst to facilitate the commercialization of acidic water electrolyzers. In this context, Tiwari *et al.* presented t-phase ruthenium oxide atomic layers implanted on $Mo_2TiC_2T_x$ MXene (RAL-M) as an exemplary electrocatalyst for OER in acidic media. RAL-M demonstrates outstanding mass activity (6.2 A mg^{-1}), excellent turnover frequency (TOF; 2.4 s^{-1}), and negligible durability loss even after 22 hours in a two-electrode cell configuration. Notably, the mass activity and TOF of RAL-M surpass industrial electrocatalysts (RuO_2-Premetek Co. and RuO_2-Sigma-Aldrich) by 150 times and 540 times, respectively, at pH 0.48. The prepared electrocatalyst showed an overpotential of 390 mV and a Tafel slope of 50.4 mV dec^{-1}. Computational calculations showed that the ruthenium active sites in RAL-M exhibit a strong affinity for oxygen species (*e.g.*, OH*, O*, and OOH*), facilitating water dissociation and favoring both the adsorbate evolution and lattice oxygen mechanistic pathways to expedite the OER. Density Functional Theory (DFT) outcomes indicated that the most advantageous mechanism for the Oxygen Evolution Reaction (OER) over the Ruthenium (Ru) active sites is the Anion Exchange Mechanism (AEM).[95]

MXene-based hybrid architectures as bifunctional electrocatalyst

Efforts are being carried out by researchers to synthesize non noble metal based electrocatalyst being highly conductive, cost-effective, durable, efficient and bifunctional that can couple both HER and OER in the same media.[97] Bifunctional catalysts exhibit higher activity compared to unifunctional catalysts since optimal conditions differ for each activity, and they also reduce setup time for instrumentation.[98] To address these challenges, extensive efforts have been devoted to the development of electrode materials such as carbides, phosphides, nitrides, carbon nitrides, metal oxides, and transition metal dichalcogenides (TMDCs).[99] Bifunctional catalysts, however, face two main issues: poor conductivity leading to high mass loading and electrode thickening, resulting in decreased activity, as well as the instability of NPM-based electrolytes in aqueous solutions. The recent discovery of 2D MXenes, characterized by high conductivity and rich surface chemistry, offers a potential solution to overcome these challenges.

Zahra *et al.* synthesized $Mo_2T_iC_2T_x$ and $Mo_2Ti_2C_3T_x$ double transition metal carbides as bifunctional catalysts based on non-precious metals (NPM) for overall water splitting in alkaline media.[100] The catalytic activity was evaluated using linear sweep voltammetry (LSV), which demonstrated the remarkable performance of $Mo_2TiC_2T_x$ and $Mo_2Ti_2C_3T_x$ in terms of high hydrogen evolution reaction (HER) activity. Specifically, $Mo_2TiC_2T_x$ exhibited an overpotential of 34 mV, while $Mo_2Ti_2C_3T_x$ showed an overpotential of 51 mV, to reach current density of 10 mA cm^{-2}. The stability of the catalyst was estimated through a long-term durability test lasting 24 hours, and it exhibited excellent stability with a current retention of 83%. A comparison between the $Mo_2TiC_2T_x$ and $Mo_2Ti_2C_3T_x$ catalysts revealed that the $Mo_2TiC_2T_x$ catalyst outperformed the $Mo_2Ti_2C_3T_x$ catalyst due to its lower charge transfer resistance. Furthermore, $Mo_2TiC_2T_x$ showed a lower overpotential of 320 mV@η_{10} and a Tafel slope of 86 mV dec^{-1}, whereas $Mo_2Ti_2C_3T_x$ exhibits a higher overpotential of 470 mV dec^{-1} and a relatively greater Tafel slope of 145 mV dec^{-1}. This significant difference in performance can be attributed to the better conductivity and metallic nature of $Mo_2TiC_2T_x$ in contrast to the semiconducting behavior of $Mo_2Ti_2C_3T_x$, leading to enhanced OER activity assisted by faster diffusion kinetics.[100]

In another study, Ashraf *et al.* presented the synthesis of a Ti_3C_2@MoO_3 nanocomposite through a hydrothermal method, resulting in an electrocatalyst with enhanced activity and stability for overall water splitting. In this nanocomposite, Ti_3C_2 served as a conductive material, promoting rapid electron transfer, while MoO_3 contributed to long-term stability by preventing the restacking of Ti_3C_2 nanosheets. The nanocomposite exhibited superior HER and OER activity, with a low overpotential of 91 mV and 190 mV respectively at current density of 10 mA cm^{-2}. Furthermore, the nanocomposite exhibits long-term durability, lasting for 50 hours. The strong electronic coupling effect between Ti_3C_2 MXene and MoO_3 nanobelts facilitates the kinetics of the HER and OER reactions. LSV polarization curve was used to evaluate the OER performance of Ti_3C_2 MXene, MoO_3 nanobelts, and Ti_3C_2@MoO_3 composites with different compositions (50%, 75%, and 25% of MoO_3). The results revealed that Ti_3C_2 exhibited moderate OER activity, indicating the need for further improvement to reach the standard activity level. Ti_3C_2 MXene and MoO_3 nanobelts exhibit high overpotentials of 450 mV and 320 mV, respectively, to achieve a current density of 10 mA cm^{-2}. However, when combined in Ti_3C_2@MoO_3 composites with different compositions (50%, 75%, and 25% of MoO_3), the overpotential values decrease. Ti_3C_2@MoO_3 (50%) shows the lowest overpotential of 190 mV, while Ti_3C_2@MoO_3 (75%) and Ti_3C_2@MoO_3 (25%) showed larger overpotentials of 312 mV and 270 mV, respectively. This improvement in activity was attributed to the synergistic effect between the two metals and the development of an excellent conductive network between Ti_3C_2 MXene and MoO_3 nanobelts. The superior overpotential observed in Ti_3C_2@MoO_3 (50%) can be attributed to its larger surface area as compared to Ti_3C_2@MoO_3 (75%) and Ti_3C_2@MoO_3 (25%). The nanocomposites consisting of Ti_3C_2 MXene, MoO_3 nanobelts, and their combinations (Ti_3C_2@MoO_3 (50%), Ti_3C_2@MoO_3 (75%), and Ti_3C_2@MoO_3 (25%)) were evaluated as catalysts for the hydrogen evolution reaction (HER) on nickel foam support. These nanocomposites exhibited remarkably low onset potentials for HER. Specifically, Ti_3C_2@MoO_3 (50%) demonstrated an overpotential of 91 mV at a current density of 10 mA cm^{-2}, displaying excellent catalytic performance with higher current densities achieved at more negative potentials. In comparison, Ti_3C_2@MoO_3 (75%), Ti_3C_2@MoO_3 (25%), MoO_3, and Ti_3C_2 exhibited higher overpotentials of 118 mV (at 10 mA), 110 mV (at 10 mA), 192 mV (at 10 mA), and 152 mV (at 5 mA), respectively. Additionally, Ti_3C_2@MoO3 (50%) demonstrated a low Tafel slope of 34 mV dec^{-1}, outperforming Ti_3C_2@MoO_3 (75%) (67 mV dec^{-1}), Ti_3C_2@MoO_3 (25%) (53 mV dec^{-1}), MoO_3 (76 mV dec^{-1}), and Ti_3C_2 (119 mV dec^{-1}) nanobelts.[101]

Rasheed *et al.* employed a novel acid-free wet chemical method to synthesize MXene and its composites with $CoNiFe_2O_4$ for efficient overall water splitting SEM images are shown in Fig. 13, (a) Pure MAX, (b) MXene, (c) $CoNiFe_2O_4$ NPs, and (d) $CoNiFe_2O_4$/MXene composites. A layer-by-layer (LBL) assembly was adopted to construct a $CoNiFe_2O_4$/MXene-based 2D/NPs/2D network that effectively prevented restacking of MXene flakes. The incorporating nanoparticles (NPs) *via* LBL approach, resulted in a high surface area and numerous active sites for water splitting. The fabricated catalyst exhibited outstanding performance with low overpotentials of 149 mV and 17 mV at a current density of 10 mA cm^{-2} for oxygen evolution reaction (OER) and hydrogen evolution reaction (HER), respectively. Moreover, Tafel slopes of 36 mV dec^{-1} for HER and 45 mV dec^{-1} for OER were achieved demonstrating favorable kinetics. The catalyst also revealed remarkable electrochemical stability for up to 100 hours, exceeding many similar catalysts reported in recent literature.[23]

In general, the MAX phase serves as the initial compound, and the production of MXenes involves the targeted removal of A element layers from the MAX phase through the use of F-containing acids or salts like HF, NH_4HF_2, or LiF/HCl, with A representing Al or Si. MXenes generated using HF acid have drawbacks, as HF can break the MXene sheets and, being a potent acid, poses health and environmental risks. Therefore, MXenes free of HF present a more advantageous alternative to conventional HF-based MXenes. Sarfraz *et al.* synthesized environmentally friendly MXene with Cl termination by subjecting MAX phase and copper chloride to thermal treatment at 550 °C for 5–6 hours in a tube furnace, conducted under an inert Ar gas atmosphere.

In this study, authors reported the synthesis of CuS nanoparticles composite with 2D environmentally friendly, HF-free Cl-terminated MXene ($Ti_3C_2Cl_2$) sheets using the hydrothermal method, establishing an effective electrocatalyst for the hydrogen evolution reaction (HER) and overall water splitting. The CuS/$Ti_3C_2Cl_2$ composite demonstrated an overpotential of 163 mV and a Tafel slope of 77 mV dec^{-1} at 10 mA cm^{-2} for HER. For the oxygen evolution reaction (OER), CuS/$Ti_3C_2Cl_2$ displayed an overpotential of 334 mV at 50 mA cm^{-2} with a Tafel slope of 42 mV dec^{-1}. Additionally, the CuS/$Ti_3C_2Cl_2$ electrolyzer, when assembled, achieved a current density of 20 mA cm^{-2} at 1.87 V for overall water splitting. The CuS/$Ti_3C_2Cl_2$ electrocatalyst exhibited remarkable stability, retaining 96% of its initial value for approximately 48 hours at a current density of 100 mA cm^{-2}. The synthesis of CuS/$Ti_3C_2Cl_2$ expands the applications of MXene/metal sulfides in efficient bifunctional electrocatalysis for alkaline water splitting. The high performance of the electrocatalyst was attributed to the highly crystalline structure of Cl-terminated MXene synthesized at high temperature and the presence of CuS nanoparticles between the layers of MXenes.[102]

Jang *et al.* employed a hydrothermal reaction to immobilize nickel-iron sulphide (NiFeS) nanosheets on Ti_3C_2 MXene-decorated nickel foam (Ti_3C_2 MXene/NF), to create NiFeS@Ti_3C_2 MXene/NF. The morphological features of NiFeS, along with its interactions with Ti_3C_2 MXene, led to electronic coupling that optimized the adsorption energies of water, protons, and oxygen atoms for both the Hydrogen Evolution Reaction (HER) at 180 mV@20 mA cm^{-2} and the Oxygen Evolution Reaction (OER) at 290 mV@20 mA cm^{-2}. The NiFeS@Ti_3C_2 MXene/NF catalyst demonstrated excellent water splitting performance in an alkaline membrane water electrolyzer, achieving a current density (j) of 401 mA cm^{-2} at 1.85 V with a 67.65% cell efficiency, a performance comparable to Pt/C||RuO_2 cells. From a commercial standpoint, electrolyzers

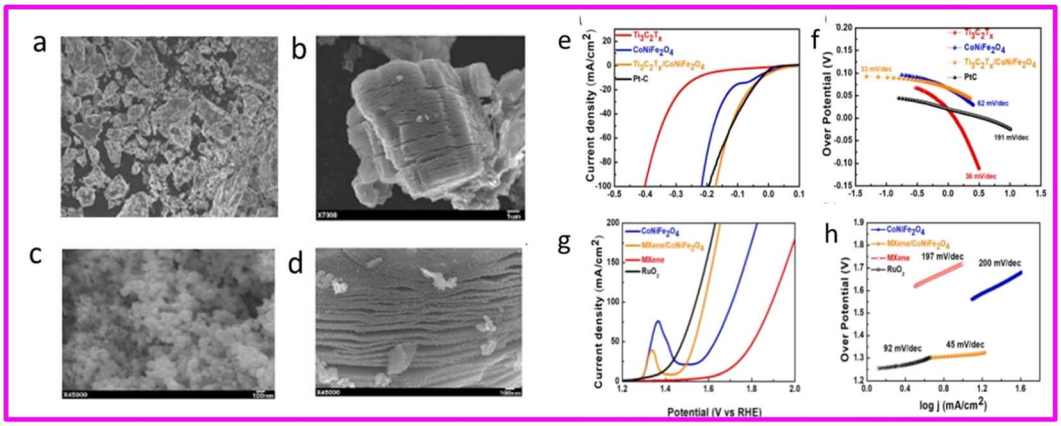

Fig. 13 SEM images that show (a) pure MAX, (b) MXene, (c) $CoNiFe_2O_4$ NPs, (d) $CoNiFe_2O_4$/MXene composites, electrocatalytic HER performance of $CoNiFe_2O_4$, MXene, $CoNiFe_2O_4$/MXene composites, and commercial PtC. (e) LSV curves, (f) Tafel slop, electrocatalytic HER performance of $CoNiFe_2O_4$, MXene, $CoNiFe_2O_4$/MXene composites, and commercial PtC. (g) LSV curves, (h) Tafel slope. Reproduced with permission.[23]

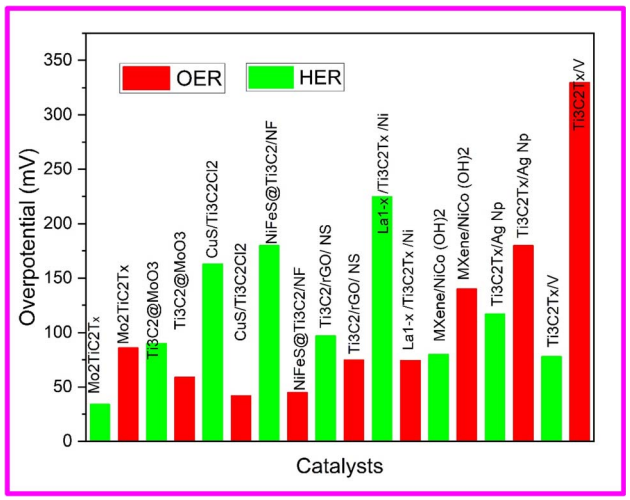

Fig. 14 Comparison HER and OER performance of bifunctional electrocatalysts.

stand out due to their low catalyst loading (approximately 1.25 mg cm^{-2}) and low operating temperatures (50 °C), resulting in reduced capital and operating costs. These findings contribute to the advancement of commercial green hydrogen production and present a viable alternative to Proton Exchange Membrane Water Electrolysis (PEMWE).[103]

In another study, Khadija *et al.* devised innovative three-dimensional (3D) Ti_3C_2 MXene/reduced graphene oxide (rGO) composite aerogels (MGA) incorporating octahedron-like $NiSe_2$ (NS) with varying mass loadings of MXene (20 wt% and 40 wt%). The resulting aerogels form a cellular lattice-like network, significantly enhanced the contact area between the active material and electrolyte. The 3D spongy scaffold of MGA increased the mass diffusion rate, while the excellent electrical conductivity of MXene and rGO facilitated rapid charge transport during electrochemical tests, leading to superior water splitting performances. As a bifunctional electrocatalyst, NSMGA-40 required a low overpotential of 97 mV and 262 mV to reach 10 mA cm^{-2} for hydrogen evolution reaction (HER) and oxygen evolution reaction (OER) activities, respectively, in alkaline media. The Tafel slopes are as small as 89 mV dec^{-1} (HER) and 75 mV dec^{-1} (OER), indicating accelerated electron-transfer kinetics. Moreover, in both cases, the NSMGA-40 electrocatalyst demonstrates long-term stability over a 10 hour test. Consequently, the results highlight the potential of structural and componential engineering to maximize synergistic effects from Ti_3C_2 MXene, rGO, and NS. The fabricated aerogels served as a valuable reference for the design of 3D multicomponent electrode materials in energy storage and conversion applications.[104]

The strategic design of cost-effective and high-performance electrocatalytic systems for water splitting holds significant importance in promoting energy and environmental sustainability. The development of a sustainable energy conversion-assisted electrocatalytic process offers a promising and innovative approach to enhance its overall performance. In this context, a self-sustained water-splitting system was designed by Lu *et al.*, originating from the heterostructure of perovskite oxide with 2D $Ti_3C_2T_x$ MXene on Ni foam ($La_{1-x}Sr_xCoO_3/Ti_3C_2T_x$ MXene/Ni). This system demonstrated elevated activity for solar-powered water evaporation and simultaneous electrocatalytic water splitting. The all-in-one interfacial electrocatalyst displays notably enhanced oxygen evolution reaction (OER) performance, featuring a low overpotential of 279 mV at 10 mA cm^{-2} and a minimal Tafel slope of 74.3 mV dec^{-1}, surpassing the performance of previously reported perovskite oxide-based electrocatalysts.

The 2D heterostructure of $La_{0.9}Sr_{0.1}CoO_3/Ti_3C_2T_x$ MXene on Ni foam (LMN) served a dual role by functioning as a photothermal solar evaporator and an effective electrocatalyst for both the oxygen evolution reaction (OER) and hydrogen evolution reaction (HER). The improved catalytic capabilities of LMN under solar illumination arise from the facilitated electron transfer within the heterogeneous catalyst and localized

Table 3 Comparison of electrocatalytic performance of bifunctional electrocatalysts

		HER		OER			
Catalyst	Electrolyte	Overpotential (mV)@10 mA cm^{-2}	Tafel slope (mV dec^{-1})	Overpotential (mV) @10 mA cm^{-2}	Tafel slope (mV dec^{-1})	Scan rate (mV s^{-1})	Ref.
$Mo_2TiC_2T_x$	1 M KOH	34	30	320	86	10	99
Ti_3C_2@MoO_3	1 M KOH	90	34	190	59	10	100
CuS/$Ti_3C_2Cl_2$	1 M KOH	163	77	334	42	10	101
NiFeS@Ti_3C_2/NF	1 M KOH	180	165	290	45	10	98
Ti_3C_2/rGO/NS	1 M KOH	97	89	262	75	—	103
$La_{1-x}Sr_xCoO_3/Ti_3C_2T_x$/Ni	1 M KOH	225	96.3	279	74.3	5	104
MXene/$NiCo(OH)_2$	1 M KOH	80	90	300	140	10	105
$Ti_3C_2T_x$/Ag Np	0.5 M H_2SO_4	117	270	250	180	10	57
$Ti_3C_2T_x$/V		78	90	175	330	—	106

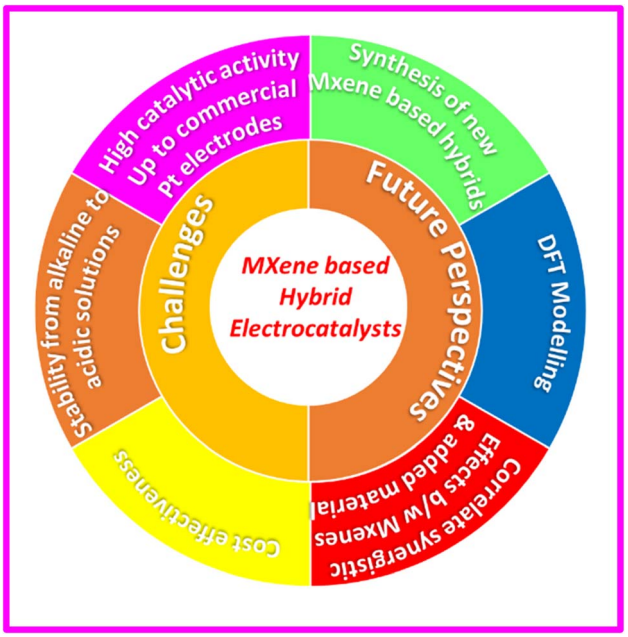

Fig. 15 Schematics describing the challenges and future prospects of MXene based hybrids.

interfacial effects induced by interfacial solar evaporation, as verified through both experimental observations and theoretical analyses. Density functional theory calculations indicate that integrating $La_{0.9}Sr_{0.1}CoO_3$ with $Ti_3C_2T_x$ MXene can reduce the energy barrier for electron transfer and decrease the OER overpotential. Additionally, COMSOL simulations reveal that interfacial solar evaporation induces OH^- enrichment near the catalyst surfaces and enhances convection flow above the catalysts, effectively expelling the generated gas and significantly accelerating the kinetics of electrocatalytic water splitting.[105]

In recent investigations, there has been a prolonged focus on utilizing low-cost and readily available nickel cobalt hydroxides ($NiCo(OH)_2$) in layered double hydroxides (LDHs). However, the tendency of these flakes to aggregate and their structural instability has resulted in fewer accessible active sites, leading to inadequate electrical conductivity. This limitation hampers their effectiveness as electrocatalysts. Navyjyoti *et al.* employed a one-step hydrothermal method to create MXene-supported $NiCo(OH)_2$ samples, varying the Co ratios, to address these issues. These samples exhibited an increased surface area and numerous active sites, enhancing their electrochemical activity. Specifically, the electrocatalyst NCM-1.2, with a Ni : Co ratio of 1 : 1.2, demonstrated compelling performance with overpotential of 80 mV for the HER and 300 mV for OER at current density of 10 mA cm^{-2} and Tafel slope of 90 mV dec^{-1} and 140 mV dec^{-1} respectively. The high electrocatalytic activity of NCM-1.2 can be attributed to active redox couples (Ni^{2+} and Co^{2+}), improved accessibility of active sites (Ni^{2+} for HER and Co^{3+} for OER), and reduced interfacial charge transfer resistance.[106]

The 2D MXene, $Ti_3C_2T_x$, has been identified as a promising candidate for catalyzing the hydrogen evolution reaction (HER) due to its intriguing physiochemical properties. However, its potential in the field of the oxygen evolution reaction (OER) remains unexplored due to slow kinetics and high overpotentials. In a study, Sharma *et al.* introduced a simple method to simultaneously enhance the bifunctionality of MXene by adjusting the surface-exposed Ti species (Ti^{4+} and Ti^{2+}) to act as catalytic centers through the *in situ* growth of silver nanoparticles (AgNPs). The incorporation of AgNPs alters the electronic environment of electroactive sites, optimizing the adsorption and desorption energies of chemisorbed reaction intermediates *via* interfacial charge transfer. Additionally, this research sheds light on the detailed mechanism explaining the decline in electrochemical performance when AgNPs agglomerate, as confirmed by TEM and XPS results. The optimized electrode demonstrated a current density of 10 mA cm^{-2} at overpotentials of 0.117 V and 0.25 V for HER and OER, respectively, in 0.5 M H_2SO_4. Consequently, this study presents an innovative strategy for exploring the surface Ti species of MXene as effective electroactive sites, leading to significantly improved kinetics in both HER and OER reactions.[57]

MXene nanosheets aggregation and their thermodynamic instability significantly diminish active sites, leading to a decline in overall water-splitting efficiency. To address these challenges, surface engineering approaches involving the introduction of large-sized dopants have been recognized. In this context, Sharma *et al.* proposed a strategy for tuning the

MXene surface through substitutional vanadium doping, introducing additional electrochemically active surface sites (V^{1+}, V^{2+}, V^{3+}, V^{4+}, and V^{5+}) alongside the inherent MXene sites (Ti^{2+}, Ti^{3+}, and Ti^{4+}). This doping also hinders the unavoidable self-restacking and minimizes inherent aqueous oxidation. Vanadium doping facilitates the creation of numerous intimate heterointerface networks, promoting electronic redistribution on the conducting surface of MXene. Consequently, highly active sites, primarily with low-valence (V^{1+} and Ti^{2+}) and high-valence (V^{5+} and Ti^{4+}), are generated for the hydrogen evolution reaction (HER) and oxygen evolution reaction (OER), respectively. The optimized sample, benefiting from synergistic surface features, demonstrates superior bifunctionality and long-term durability in driving both HER and OER with overpotentials of 78 (90 mV dec^{-1}) and 175 mV (330 mV dec^{-1}), respectively. Moreover, a water-splitting system assembled with this material exhibited a low cell voltage of 1.48 V. Thus, this study provides crucial insights for significantly and simultaneously enhancing the surface utilization of MXene, ensuring abundant electrochemically active sites and paving the way for the design of high-performance water-splitting electrolyzers.[107] Fig. 14 show the graphical comparison overpotentials for HER and OER of bifunctional electrocatalysts based on MXenes and their hybrids (Table 3).

Conclusions

This review provides a summary discussion on recent developments in electrocatalytic hydrogen and oxygen evolution reactions, with a specific focus on 2D layered MXenes and their hybrid architectures. The principal objective of this research area is to substitute costly and quickly depleting precious metal-based electrocatalysts. The reaction kinetics of HER, OER and overall water splitting are mainly controlled by structure and properties of the electrocatalyst which is one of the crucial components of the water splitting system. Excellent electrocatalytic performance have been demonstrated by the electrocatalyst high electrical conductivity, abundant active sites and very large surface area are the key requirements of an electrocatalyst to exhibit excellent water splitting activity. MXenes, 2D transition metal carbides, nitrides and carbon nitrides have shown all the aforementioned salient features of good electrocatalyst.

This review highlights the electrocatalytic potential of MXenes and their hybrids with various materials such as metal organic frameworks, layered double hydroxides, transition metal dichalcogenides, offering both excellent performance for HER, OER and overall water splitting along with long term stability and recyclability.

Challenges and future perspectives

Use of new MXenes

Numerous investigations have indicated that nitride MXenes present several potential benefits compared to their carbide counterparts, including elevated conductivity and stability in aqueous environments. While carbide MXenes have been extensively studied for electrocatalytic water splitting, there are only a few experimental reports on nitride MXenes. The crucial research emphasis should center on identifying appropriate preparation methods and understanding the roles of nitride MXenes in electrocatalytic water splitting. Additionally, there is a need to diversify the types of MXenes developed to broaden the MXene family. The electrocatalytic potential of double transition metal MXenes and their hybrids has not been fully explored yet which demands more focus of researchers. Fig. 15 shows schematics describing the challenges and future prospects of MXene based hybrids.[107]

Synthesis of new hybrids

Although several investigations have been performed in the development and application of MXene based hybrids for energy conversion reactions, many points need to be addressed systematically to solve challenges ahead in this research area. The widespread applications of MXene based electrocatalysts for water splitting requires the development of a scalable method for synthesis of MXenes and hybrid materials without compromising on the qualities and properties of the electrocatalyst. The synergistic effects between MXenes and material alloying with them are very complex and are of vital importance to understand the role of heterointerface in catalytic activity. So, more attention must be paid to have deeper understanding of structure–property relationship of MXene based hybrid systems by the development of *in situ* characterization techniques to observe the real time structural reconstruction. Density functional theoretical calculations with accurate models should be employed to clearly understand the reaction mechanism of binary and ternary composite electrocatalysts that will help to synthesize better MXene based hybrids for water electrolysis.

Instability issue of MXenes and its hybrids

The recyclability and long-term stability of MXene based electrocatalyst have been affected by restacking and agglomeration of MXene flakes. This problem can be avoided by alloying MXenes with various materials including nanoparticles, nanoclusters, quantum dots and 2D layered materials as well. Primarily, the catalysts for Oxygen Evolution Reaction (OER), and Hydrogen Evolution Reaction (HER) need to operate effectively in both highly acidic and alkaline environments to reduce overpotentials. This poses a significant challenge for many non-noble metal electrocatalysts because they may become inactive or unstable in extremely acidic or alkaline conditions. The interface chemistry of an electrocatalyst plays an important role in order to optimize their electrocatalytic activity and stability.

Reduction in overpotential

While notable advancements have been made in minimizing the overpotential of MXene based hybrid architectures in case of HER, OER and overall water splitting. Still, numerous unresolved issues require thorough investigation.

Schottky junctions formed by combining MXene with other materials can also be used to decrease the overpotential of the electrocatalysts.

The sluggish kinetics of the OER half-reaction causes more overpotential in the entire water-splitting process. To tackle this issue, a good approach is to exchange the OER reaction with other reactions that have lower oxidation potential and faster reaction rates. This may help in lowering the overpotential for producing hydrogen through HER.

In particular, combining hydrogen evolution reaction (HER) with certain organic reactions generating valuable chemicals can decrease overpotential and, consequently, reduce the overall cost of producing hydrogen. While this approach hasn't been implemented in one-dimensional MXene based hybrid architectures yet, we suggest that it could be a successful method to diminish overpotential in these structures for solar hydrogen production.

There are several other ways to decrease the overall overpotential and ohmic resistance in water electrolysis, in addition to optimization of the electrode materials. For example, approaches to enhance electrolyte movement through different means, such as utilizing gravity, employing mechanical stirring and magnetic fields, must also be adopted. By promoting better mass transfer and reducing resistance during the electrochemical process, these tactics aim to improve the efficiency of water electrolysis.

Integration of various energy conversion systems

More efficient, versatile and sustainable tandem cell based on MXene can be made by integrating the water splitting cell with other energy conversion technologies such as photovoltaics and thermoelectrics. This integration allows will result in a more comprehensive energy conversion system, possibly enhancing overall efficiency and contributing to the advancement of multifunctional devices for sustainable energy applications. Tandem cell can deliver a nonstop and stable power output, even when one specific energy source is not available or is intermittently available leading to cost effective energy production.

Large scale application

As electrochemical energy conversion reactions become more technically achievable and economically practical, the need for large-scale catalyst and electrolyzer manufacturing methods will rise to fulfill the demand for sustainable chemical and fuel production. Carbon-Ukraine Ltd., in partnership with the Materials Research Centre in Ukraine, provides extensive MXene synthesis services. They utilize specially designed etching reactors capable of producing 100 grams of $Ti_3C_2T_x$ in each batch, which holds a promise for future industrial scale synthesis of MXene based electrocatalyst.[108]

The future scaling of green hydrogen production faces challenges related to environmental impacts, specifically concerning material usage and land transformation. Previous approaches to designing hydrogen production configurations have employed static sizing methodologies, but there is a recognized need to optimize these systems based on site-specific conditions. This optimization aims to minimize both the production costs of hydrogen and the associated environmental burdens, emphasizing a more sustainable and efficient approach to large-scale green hydrogen production.[109]

Comparison of electrocatalysis with other technologies

Electrocatalytic water splitting is a green and established approach that involves the generation of hydrogen and oxygen through. Despite the potential advantages of electrocatalytic hydrogen production, it currently faces several significant challenges that distance it from other state-of-the-art hydrogen production technologies. One key challenge lies in the scalability and cost-effectiveness of electrocatalysis for hydrogen production. However, a drawback is the high cost of electricity, constituting around 80% of the operation cost as compared with other methods such as steam methane reforming (SMR). Currently, hydrogen production from electrolysis has its share of only 4% and 96% of hydrogen produced in global market comes from hydrocarbons. Therefore, it is imperative to decrease the costs and enhance the efficiency of electrocatalysis through the optimization of reactor design, catalyst loading, and operating conditions. Integration of electrocatalysis with other renewable energy sources and energy storage systems is also crucial. Moreover, there is a need for the establishment of policy and regulatory frameworks that can facilitate the deployment of electrocatalysis technologies and offer incentives for the utilization of renewable energy sources.

Use of artificial intelligence

Computational approaches grounded in density functional theory have effectively predicted catalyst activity, elucidated catalytic phenomena, and identified novel high-performance catalysts. Furthermore, the relatively recent emergence of artificial intelligence (AI) techniques is gradually finding application in materials and chemistry research domains. The growing significance of these advanced computational tools in scientific inquiry is increasingly apparent. However, their utilization in electrocatalytic water splitting research remains limited. It is conceivable that the advancement and optimal use of high-performance MXene based hybrid electrocatalysts could be notably enhanced by incorporating and fully leveraging theoretical computing and AI technologies.

Conflicts of interest

There are no conflicts to declare.

Acknowledgements

The authors thank the Higher Education Commission (HEC) of Pakistan for providing research funding under the Project No. 20-14784/NRPU/R&D/HEC/2021.

References

1 W. Zhu, L. Yang, F. Liu, Z. Si, M. Huo, Z. Li and Z. Chen, Metal Ni nanoparticles in-situ anchored on CdS nanowires as effective cocatalyst for boosting the

photocatalytic H2 production and degradation activity, *J. Alloys Compd.*, 2024, **973**, 172747.
2 X. Feng, L. Sun, W. Wang, Y. Zhao and J. Shi, Construction of CdS@ZnO core–shell nanorod arrays by atomic layer deposition for efficient photoelectrochemical H_2 evolution, *Sep. Purif. Technol.*, 2023, **324**, 124520.
3 C. Si, *et al.*, Recent Advances in Perovskite Catalysts for Efficient Overall Water Splitting, *Catalysts*, 2022, **12**(6), 601.
4 L.-N. Shi, *et al.*, Towards high-performance electrocatalysts: Activity optimization strategy of 2D MXenes-based nanomaterials for water-splitting, *Coord. Chem. Rev.*, 2022, **469**, 214668.
5 M. Zeng and Y. Li, Recent advances in heterogeneous electrocatalysts for the hydrogen evolution reaction, *J. Mater. Chem. A*, 2015, **3**(29), 14942–14962.
6 S. A. Zahra and S. Rizwan, MWCNT-modified MXene as cost-effective efficient bifunctional catalyst for overall water splitting, *RSC Adv.*, 2022, **12**(14), 8405–8413.
7 F. Almomani, *et al.*, A comprehensive review of hydrogen generation by water splitting using 2D nanomaterials: Photo *vs.* electro-catalysis, *Fuel*, 2023, **332**, 125905.
8 A. Raveendran, M. Chandran and R. Dhanusuraman, A comprehensive review on the electrochemical parameters and recent material development of electrochemical water splitting electrocatalysts, *RSC Adv.*, 2023, **13**(6), 3843–3876.
9 Y. Wen, *et al.*, 2D TiVCT$_x$ layered nanosheets grown on nickel foam as highly efficient electrocatalysts for the hydrogen evolution reaction, *RSC Adv.*, 2022, **12**(36), 23584–23594.
10 I. Dincer and C. Acar, Review and evaluation of hydrogen production methods for better sustainability, *Int. J. Hydrogen Energy*, 2015, **40**(34), 11094–11111.
11 C. Wang, P. Shi, C. Guo, R. Guo and J. Qiu, $CuCo_2O_4$/CF cathode with bifunctional and dual reaction centers exhibits high RhB degradation in electro-Fenton systems, *J. Electroanal. Chem.*, 2024, 118072.
12 Z. Y. Yu, *et al.*, Clean and affordable hydrogen fuel from alkaline water splitting: past, recent progress, and future prospects, *Adv. Mater.*, 2021, **33**(31), 2007100.
13 A. Karmakar, *et al.*, Surface Decoration of DNA-Aided Amorphous Cobalt Hydroxide *via* Ag^+ Ions as Binder-Free Electrodes toward Electrochemical Oxygen Evolution Reaction, *Inorg. Chem.*, 2021, **60**(4), 2680–2693.
14 M. Zubair, *et al.*, 2D MXenes and their heterostructures for HER, OER and overall water splitting: a review, *Int. J. Hydrogen Energy*, 2022, **47**(5), 2794–2818.
15 Y. Li, *et al.*, Recent advances on water-splitting electrocatalysis mediated by noble-metal-based nanostructured materials, *Adv. Energy Mater.*, 2020, **10**(11), 1903120.
16 S. Chandrasekaran, *et al.*, Recent advances in metal sulfides: from controlled fabrication to electrocatalytic, photocatalytic and photoelectrochemical water splitting and beyond, *Chem. Soc. Rev.*, 2019, **48**(15), 4178–4280.
17 C. Wang, *et al.*, Iridium-based catalysts for solid polymer electrolyte electrocatalytic water splitting, *ChemSusChem*, 2019, **12**(8), 1576–1590.
18 N. Wang, *et al.*, Graphene composites with Ru-RuO_2 heterostructures: highly efficient Mott–Schottky-type electrocatalysts for pH-universal water splitting and flexible zinc–air batteries, *Appl. Catal., B*, 2022, **302**, 120838.
19 C. Li and J.-B. Baek, Recent advances in noble metal (Pt, Ru, and Ir)-based electrocatalysts for efficient hydrogen evolution reaction, *ACS Omega*, 2019, **5**(1), 31–40.
20 R. Djara, *et al.*, Iridium and ruthenium modified polyaniline polymer leads to nanostructured electrocatalysts with high performance regarding water splitting, *Polymers*, 2021, **13**(2), 190.
21 J. Yu, *et al.*, Ultrafine ruthenium-iridium alloy nanoparticles well-dispersed on N-rich carbon frameworks as efficient hydrogen-generation electrocatalysts, *Chem. Eng. J.*, 2021, **417**, 128105.
22 S. Chandrasekaran, *et al.*, Developments and Perspectives on Robust Nano-and Microstructured Binder-Free Electrodes for Bifunctional Water Electrolysis and Beyond, *Adv. Energy Mater.*, 2022, **12**(23), 2200409.
23 T. Rasheed, *et al.*, Bifunctional electrocatalytic water splitting augmented by cobalt-nickel-ferrite NPs-supported fluoride-free MXene as a novel electrocatalyst, *Fuel*, 2023, **346**, 128305.
24 Z. Lv, *et al.*, Designed synthesis of WC-based nanocomposites as low-cost, efficient and stable electrocatalysts for the hydrogen evolution reaction, *CrystEngComm*, 2020, **22**(27), 4580–4590.
25 Y. Tang, *et al.*, MXene nanoarchitectonics: defect-engineered 2D MXenes towards enhanced electrochemical water splitting, *Adv. Energy Mater.*, 2022, **12**(12), 2103867.
26 H. Sun, *et al.*, Self-supported transition-metal-based electrocatalysts for hydrogen and oxygen evolution, *Adv. Mater.*, 2020, **32**(3), 1806326.
27 K. R. G. Lim, *et al.*, Rational design of two-dimensional transition metal carbide/nitride (MXene) hybrids and nanocomposites for catalytic energy storage and conversion, *ACS Nano*, 2020, **14**(9), 10834–10864.
28 D. Zhou, *et al.*, Recent advances in non-precious metal-based electrodes for alkaline water electrolysis, *ChemNanoMat*, 2020, **6**(3), 336–355.
29 X. Cao, T. Wang and L. Jiao, Transition-metal (Fe, Co, and Ni)-based nanofiber electrocatalysts for water splitting, *Adv. Fiber Mater.*, 2021, 1–19.
30 B. R. Wygant, K. Kawashima and C. B. Mullins, Catalyst or precatalyst? The effect of oxidation on transition metal carbide, pnictide, and chalcogenide oxygen evolution catalysts, *ACS Energy Lett.*, 2018, **3**(12), 2956–2966.
31 K. N. Dinh, *et al.*, Nanostructured metallic transition metal carbides, nitrides, phosphides, and borides for energy storage and conversion, *Nano Today*, 2019, **25**, 99–121.
32 S. Bai, *et al.*, Recent advances of MXenes as electrocatalysts for hydrogen evolution reaction, *npj 2D Mater. Appl.*, 2021, **5**(1), 78.
33 H. Zhang, *et al.*, Bifunctional heterostructured transition metal phosphides for efficient electrochemical water splitting, *Adv. Funct. Mater.*, 2020, **30**(34), 2003261.

34 X.-P. Li, *et al.*, Transition metal-based electrocatalysts for overall water splitting, *Chin. Chem. Lett.*, 2021, **32**(9), 2597–2616.
35 B. Anasori and Y. Gogotsi, MXenes: trends, growth, and future directions, *Graphene 2D Nanomater.*, 2022, 1–5.
36 A. VahidMohammadi, J. Rosen and Y. Gogotsi, The world of two-dimensional carbides and nitrides (MXenes), *Science*, 2021, **372**(6547), eabf1581.
37 Z. Haider, *et al.*, Ag Nanoparticle-Decorated V_2CTx MXene Nanosheets as Catalysts for Water Splitting, *ACS Appl. Nano Mater.*, 2023, **6**(4), 2374–2384.
38 X. Zhao, B. Fan, N. Qiao, R. A. Soomro, R. Zhang and B. Xu, Stabilized $Ti_3C_2T_x$-doped 3D vesicle polypyrrole coating for efficient protection toward copper in artificial seawater, *Appl. Surf. Sci.*, 2024, **642**, 158639.
39 J. Sui, *et al.*, MXene derivatives: synthesis and applications in energy convention and storage, *RSC Adv.*, 2021, **11**(26), 16065–16082.
40 P. Urbankowski, *et al.*, Synthesis of two-dimensional titanium nitride Ti_4N_3 (MXene), *Nanoscale*, 2016, **8**(22), 11385–11391.
41 B. Anasori and Û. G. Gogotsi, *2D Metal Carbides and Nitrides (MXenes)*, Springer, 2019, vol. 2549.
42 K. R. G. Lim, *et al.*, Fundamentals of MXene synthesis, *Nat. Synth.*, 2022, **1**(8), 601–614.
43 S. A. Zahra, E. Ceesay and S. Rizwan, Zirconia-decorated V_2CT_x MXene electrodes for supercapacitors, *J. Energy Storage*, 2022, **55**, 105721.
44 A. Zaheer, *et al.*, Nickel-adsorbed two-dimensional Nb_2C MXene for enhanced energy storage applications, *RSC Adv.*, 2022, **12**(8), 4624–4634.
45 M. M. Uddin, *et al.*, Graphene-like emerging 2D materials: recent progress, challenges and future outlook, *RSC Adv.*, 2023, **13**(47), 33336–33375.
46 P. P. Michałowski, *et al.*, Oxycarbide MXenes and MAX phases identification using monoatomic layer-by-layer analysis with ultralow-energy secondary-ion mass spectrometry, *Nat. Nanotechnol.*, 2022, **17**(11), 1192–1197.
47 H. Kim, Z. Wang and H. N. Alshareef, MXetronics: electronic and photonic applications of MXenes, *Nano Energy*, 2019, **60**, 179–197.
48 A. Szuplewska, *et al.*, Future applications of MXenes in biotechnology, nanomedicine, and sensors, *Trends Biotechnol.*, 2020, **38**(3), 264–279.
49 F. Dixit, *et al.*, Application of MXenes for water treatment and energy-efficient desalination: a review, *J. Hazard. Mater.*, 2022, **423**, 127050.
50 F. Shahzad, *et al.*, Electromagnetic interference shielding with 2D transition metal carbides (MXenes), *Science*, 2016, **353**(6304), 1137–1140.
51 D. H. Ho, *et al.*, Sensing with MXenes: progress and prospects, *Adv. Mater.*, 2021, **33**(47), 2005846.
52 M. W. Hakim, *et al.*, Ni-intercalated $Mo_2TiC_2T_x$ free-standing MXene for excellent gravimetric capacitance prepared *via* electrostatic self-assembly, *J. Energy Storage*, 2023, **61**, 106662.
53 M. A. Iqbal, *et al.*, Ti_3C_2-MXene/bismuth ferrite nanohybrids for efficient degradation of organic dyes and colorless pollutants, *ACS Omega*, 2019, **4**(24), 20530–20539.
54 X. Miao, *et al.*, MXenes in tribology: current status and perspectives, *Advanced Powder Materials*, 2022, 100092.
55 A. Qadir, *et al.*, Representative 2D-material-based nanocomposites and their emerging applications: a review, *RSC Adv.*, 2021, **11**(39), 23860–23880.
56 M. M. Baig, *et al.*, 2D MXenes: synthesis, properties, and electrochemical energy storage for supercapacitors–a review, *J. Electroanal. Chem.*, 2022, **904**, 115920.
57 V. Sharma, R. Dhiman and A. Mahajan, Ti^{2+} and Ti^{4+} species enriched MXene electrocatalyst for highly efficient hydrogen evolution and oxygen evolution reaction kinetics, *Appl. Surf. Sci.*, 2023, **612**, 155883.
58 M. Chatenet, *et al.*, *Water Electrolysis: from Textbook Knowledge to the Latest Scientific Strategies and Industrial Developments.* Chemical Society Reviews, 2022.
59 J. Durst, a. Siebel, C. Simon, F. Hasché, J. Herranz and H. a. Gasteiger, *Energy Environ. Sci.*, 2014, **7**, 2255.
60 H. Schäfer, *et al.*, Electro-oxidation of a cobalt based steel in LiOH: a non-noble metal based electro-catalyst suitable for durable water-splitting in an acidic milieu, *Nanoscale*, 2017, **9**(45), 17829–17838.
61 H. Wu, *et al.*, Electrocatalytic water splitting: mechanism and electrocatalyst design, *Nano Res.*, 2023, 1–16.
62 A. Lasia, Mechanism and kinetics of the hydrogen evolution reaction, *Int. J. Hydrogen Energy*, 2019, **44**(36), 19484–19518.
63 J. Wang, *et al.*, Non-noble metal-based carbon composites in hydrogen evolution reaction: fundamentals to applications, *Adv. Mater.*, 2017, **29**(14), 1605838.
64 K. S. Lakshmi, B. Vedhanarayanan and T.-W. Lin, Electrocatalytic hydrogen and oxygen evolution reactions: role of two-dimensional layered materials and their composites, *Electrochim. Acta*, 2023, **447**, 142119.
65 Y. Wei, *et al.*, Design of efficient electrocatalysts for hydrogen evolution reaction based on 2D MXenes, *J. Energy Chem.*, 2021, **55**, 244–255.
66 Y. Zhai, *et al.*, High density and unit activity integrated in amorphous catalysts for electrochemical water splitting, *Small Struct.*, 2021, **2**(4), 2000096.
67 R. L. Doyle, *et al.*, Redox and electrochemical water splitting catalytic properties of hydrated metal oxide modified electrodes, *Phys. Chem. Chem. Phys.*, 2013, **15**(33), 13737–13783.
68 Y. Sun, *et al.*, Dynamics of Both Active Phase and Catalysis Pathway for Spinel Water-Oxidation Catalysts, *Adv. Funct. Mater.*, 2022, **32**(41), 2207116.
69 S. Chandrasekaran, *et al.*, Electronic structure engineering on two-dimensional (2D) electrocatalytic materials for oxygen reduction, oxygen evolution, and hydrogen evolution reactions, *Nano Energy*, 2020, **77**, 105080.
70 H. Xu, *et al.*, Current and future trends for spinel-type electrocatalysts in electrocatalytic oxygen evolution reaction, *Coord. Chem. Rev.*, 2023, **475**, 214869.
71 C. Ma, *et al.*, Combining MXene nanosheets with iron-based metal-organic frameworks for enhanced

electrocatalytic hydrogen evolution reaction, *Mater. Today Chem.*, 2023, **30**, 101531.

72 J. Jiang, *et al.*, Strategic design and fabrication of MXenes-Ti_3CNCl_2@CoS_2 core-shell nanostructure for high-efficiency hydrogen evolution, *Nano Res.*, 2022, **15**(7), 5977–5986.

73 K. Sharma, *et al.*, Recent progress on MXenes and MOFs hybrids: structure, synthetic strategies and catalytic water splitting, *Int. J. Hydrogen Energy*, 2023, **48**(17), 6560–6574.

74 Y. Wu, *et al.*, Boosting Hydrogen Evolution in Neutral Medium by Accelerating Water Dissociation with Ru Clusters Loaded on Mo2CTx MXene, *Adv. Funct. Mater.*, 2023, **33**(16), 2214375.

75 L. Zhang, *et al.*, Construction of Co-decorated 3D nitrogen doped-carbon nanotube/$Ti_3C_2T_x$-MXene as efficient hydrogen evolution electrocatalyst, *Int. J. Hydrogen Energy*, 2023, **48**(40), 15053–15064.

76 B. S. Reghunath, *et al.*, Hierarchical $BiFeO_3$/Cr_2CT_x MXene composite as a multifunctional catalyst for hydrogen evolution reaction and as an electrode material for energy storage devices, *Electrochim. Acta*, 2023, 142685.

77 J. Yin, *et al.*, Integration of amorphous $CoSnO_3$ onto wrinkled MXene nanosheets as efficient electrocatalysts for alkaline hydrogen evolution, *Sep. Purif. Technol.*, 2023, **308**, 122947.

78 Y. Chen, *et al.*, Interfacial engineering of Co-doped 1T-MoS_2 coupled with V_2C MXene for efficient electrocatalytic hydrogen evolution, *Chem. Eng. J.*, 2022, **450**, 138157.

79 L. Wang, *et al.*, Electronic Modulation of Metal–Organic Frameworks by Interfacial Bridging for Efficient pH-Universal Hydrogen Evolution, *Adv. Funct. Mater.*, 2023, **33**(1), 2210322.

80 L. Yan, *et al.*, Fabrication of highly efficient Rh-doped cobalt–nickel-layered double hydroxide/MXene-based electrocatalyst with rich oxygen vacancies for hydrogen evolution, *J. Colloid Interface Sci.*, 2023, **640**, 338–347.

81 B. Shen, *et al.*, 3D interweaving MXene–graphene network–confined Ni–Fe layered double hydroxide nanosheets for enhanced hydrogen evolution, *Electrochim. Acta*, 2022, **407**, 139913.

82 R. Luo, *et al.*, Facile synthesis of cobalt modified 2D titanium carbide with enhanced hydrogen evolution performance in alkaline media, *Int. J. Hydrogen Energy*, 2021, **46**(64), 32536–32545.

83 S. Ma, *et al.*, Facile fabrication of carbon fiber skeleton structure of MoS_2 supported on 2D MXene composite with highly efficient and stable hydrogen evolution reaction, *Compos. Sci. Technol.*, 2022, **222**, 109380.

84 X. Fan, *et al.*, Mechanochemical synthesis of Pt/Nb_2CT_x MXene composites for enhanced electrocatalytic hydrogen evolution, *Materials*, 2021, **14**(9), 2426.

85 C. Ma, *et al.*, *The Marriage of Hydrazone-Linked Covalent Organic Frameworks and MXene Enables Efficient Electrocatalytic Hydrogen Evolution*, Small Structures, 2023, p. 2300279.

86 S. Hussain, *et al.*, WS_2-embedded MXene/GO hybrid nanosheets as electrodes for asymmetric supercapacitors and hydrogen evolution reactions, *Chem. Eng. J.*, 2023, **452**, 139523.

87 J. Chen, *et al.*, Vertically-interlaced NiFeP/MXene electrocatalyst with tunable electronic structure for high-efficiency oxygen evolution reaction, *Sci. Bull.*, 2021, **66**(11), 1063–1072.

88 C. F. Du, *et al.*, The passive effect of MXene on electrocatalysis: a case of $Ti_3C_2T_x$/CoNi-MOF nanosheets for oxygen evolution reaction, *ChemNanoMat*, 2021, **7**(5), 539–544.

89 Y. Chen, *et al.*, V_2C MXene synergistically coupling FeNi LDH nanosheets for boosting oxygen evolution reaction, *Appl. Catal., B*, 2021, **297**, 120474.

90 C. Hao, *et al.*, Interface-coupling of CoFe-LDH on MXene as high-performance oxygen evolution catalyst, *Mater. Today Energy*, 2019, **12**, 453–462.

91 X. Zhu, *et al.*, FeP-CoP Nanocubes *In Situ* Grown on $Ti_3C_2T_x$ MXene as Efficient Electrocatalysts for the Oxygen Evolution Reaction, *Ind. Eng. Chem. Res.*, 2022, **61**(30), 10837–10845.

92 F. Yan, *et al.*, Solution Plasma-Assisted Multivariate Metal Nanoalloys Encapsulated with Carbon Dots for Efficient Oxygen Evolution Reaction, *ChemCatChem*, 2023, e202300115.

93 X. Li, *et al.*, A three-dimensional flower-like NiCo-layered double hydroxide grown on nickel foam with an MXene coating for enhanced oxygen evolution reaction electrocatalysis, *RSC Adv.*, 2021, **11**(20), 12392–12397.

94 Y. Tang, *et al.*, The effect of *in situ* nitrogen doping on the oxygen evolution reaction of MXenes, *Nanoscale Adv.*, 2020, **2**(3), 1187–1194.

95 J. N. Tiwari, *et al.*, Atomic layers of ruthenium oxide coupled with $Mo_2TiC_2T_x$ MXene for exceptionally high catalytic activity toward water oxidation, *Appl. Catal., B*, 2023, **339**, 123139.

96 S. Chandrasekaran, *et al.*, Advanced opportunities and insights on the influence of nitrogen incorporation on the physico-/electro-chemical properties of robust electrocatalysts for electrocatalytic energy conversion, *Coord. Chem. Rev.*, 2021, **449**, 214209.

97 A. I. Inamdar, *et al.*, A robust nonprecious CuFe composite as a highly efficient bifunctional catalyst for overall electrochemical water splitting, *Small*, 2020, **16**(2), 1905884.

98 H. Wang, *et al.*, Bifunctional non-noble metal oxide nanoparticle electrocatalysts through lithium-induced conversion for overall water splitting, *Nat. Commun.*, 2015, **6**(1), 7261.

99 G. Liu, *et al.*, MoS_2-Stratified CdS-$Cu_{2-x}S$ Core–Shell Nanorods for Highly Efficient Photocatalytic Hydrogen Production, *ACS Nano*, 2020, **14**(5), 5468–5479.

100 S. A. Zahra, *et al.*, Two-dimensional double transition metal carbides as superior bifunctional electrocatalysts for overall water splitting, *Electrochim. Acta*, 2022, **434**, 141257.

101 I. Ashraf, *et al.*, Fabrication of Ti_3C_2@MoO_3 nanocomposite as an electrode material for highly efficient and durable water splitting system, *Fuel*, 2021, **299**, 120928.

102 B. Sarfraz, *et al.*, Bifunctional CuS/Cl-terminated greener MXene electrocatalyst for efficient hydrogen production by water splitting, *RSC Adv.*, 2023, **13**(32), 22017–22028.
103 D. Chanda, *et al.*, Effect of the interfacial electronic coupling of nickel-iron sulfide nanosheets with layer Ti_3C_2 MXenes as efficient bifunctional electrocatalysts for anion-exchange membrane water electrolysis, *Appl. Catal., B*, 2023, **321**, 122039.
104 K. Chaudhary, *et al.*, 3D cellular lattice like-Ti_3C_2 MXene based aerogels embedded with metal selenides particles for energy storage and water splitting applications, *Fuel*, 2023, **351**, 128856.
105 Y. Lu, *et al.*, Solar-Driven Interfacial Evaporation Accelerated Electrocatalytic Water Splitting on 2D Perovskite Oxide/MXene Heterostructure, *Adv. Funct. Mater.*, 2023, **33**(21), 2215061.
106 A. K. Sharma, *et al.*, MXene supported nickel-cobalt layered double hydroxide as efficient bifunctional electrocatalyst for hydrogen and oxygen evolution reactions, *J. Alloys Compd.*, 2023, **939**, 168779.
107 V. Sharma, *et al.*, Surface engineered MXene with multi-electroactive sites for developing durable and efficient water-splitting electrolyzer, *Appl. Phys. Lett.*, 2023, **122**(19), 191601.
108 C. Tsounis, *et al.*, Advancing MXene electrocatalysts for energy conversion reactions: surface, stoichiometry, and stability, *Angew. Chem., Int. Ed.*, 2023, **62**(4), e202210828.
109 T. Terlouw, *et al.*, Large-scale hydrogen production *via* water electrolysis: a techno-economic and environmental assessment, *Energy Environ. Sci.*, 2022, **15**(9), 3583–3602.